EXPERIMENTAL INVESTIGATION OF THE OPTIMAL FILTER AS AN AREA FUNCTION PREDICTOR. SPEECH SIGNAL PROCESSING RESEARCH AT CHI

James F McGill, et al

Culler/Harrison, Incorporated

Prepared for:

Defense Supply Service
Defense Advanced Research Projects

August 1975

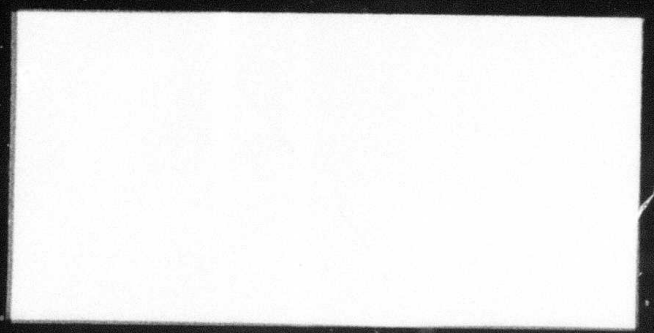

UNCLASSIFIED

SECURITY CLASSIFICATION OF THIS PAGE (When Data Entered)

REPORT DOCUMENTATION PAGE

READ INSTRUCTIONS BEFORE COMPLETING FORM

1. REPORT NUMBER CHI-QTR-102	2. GOVT ACCESSION NO.	3. RECIPIENT'S CATALOG NUMBER AD-A 014 579
4. TITLE (and Subtitle) EXPERIMENTAL INVESTIGATION OF THE OPTIMAL FILTER AS AN AREA FUNCTION PREDICTOR Quarterly Technical Report Speech Signal Processing Research at CHI		5. TYPE OF REPORT & PERIOD COVERED Quarterly Technical Report May 1975 - July 1975 6. PERFORMING ORG. REPORT NUMBER
7. AUTHOR(s) James F. McGill		8. CONTRACT OR GRANT NUMBER(s) DAHC15 73 C 0252
9. PERFORMING ORGANIZATION NAME AND ADDRESS CULLER/HARRISON, INC. 150-A Aero Camino Goleta, California 93017		10. PROGRAM ELEMENT, PROJECT, TASK AREA & WORK UNIT NUMBERS Program Code: P5P10
11. CONTROLLING OFFICE NAME AND ADDRESS Defense Supply Service - Washington Room 1D 245, The Pentagon Washington, D.C. 20310		12. REPORT DATE August 1975 13. NUMBER OF PAGES
14. MONITORING AGENCY NAME & ADDRESS(if different from Controlling Office) Defense Contract Administration Services District-VanNuys 18321 Ventura Boulevard Tarzana, California 91356		15. SECURITY CLASS. (of this report) Unclassified 15a. DECLASSIFICATION/DOWNGRADING SCHEDULE

16. DISTRIBUTION STATEMENT (of this Report)

Distribution of this document is unlimited. It may be released to the Clearinghouse, Department of Commerce for sale to the general public.

17. DISTRIBUTION STATEMENT (of the abstract entered in Block 20, if different from Report)

18. SUPPLEMENTARY NOTES

This research was supported by the Defense Advanced Research Projects Agency under ARPA Order No. 2359.

19. KEY WORDS (Continue on reverse side if necessary and identify by block number)

20. ABSTRACT (Continue on reverse side if necessary and identify by block number)

During the contract period reported here, we have investigated the optimal filter as a predictor of area functions of acoustical cavities. A model is presented which predicts spectra of circular cylindrical cavities with uniform steps in the area function. The model is used to fit data derived from the measured impulse response of such cavities. The optimal filter is found to be in error by a length factor in predicting the area function of the cavities. The accuracy of the technique is also sensitive to the spectral content of the signal near the Nyquist frequency.

DD FORM 1 JAN 73 1473 EDITION OF 1 NOV 65 IS OBSOLETE

SECURITY CLASSIFICATION OF THIS PAGE (When Data Entered)

iv

CULLER/HARRISON, INC.
150-A Aero Camino
Goleta, California 93017
(805) 968-1064

May 1975 - July 1975

EXPERIMENTAL INVESTIGATION OF THE OPTIMAL FILTER AS AN AREA FUNCTION PREDICTOR

QUARTERLY TECHNICAL REPORT
SPEECH SIGNAL PROCESSING RESEARCH AT CHI
MAY 1975 - JULY 1975

PRINCIPAL INVESTIGATOR: DR. GLEN J. CULLER

PROJECT SCIENTIST: DR. JAMES F. MCGILL

This research was supported by the Defense Advanced Research Projects Agency under ARPA Order No. 2359 Contract No. DAHC15 73 C 0252

CONTENTS

LIST OF FIGURES

SUMMARY

This report covers the work done by CHI on contract No. DAHC15 73 C 0252 during the period May 1975 to July 1975.

Under this contract we began investigating acoustical cavities as tools to verify the validity of discrete wave equations. Since we were also contracted to implement a real time LPC speech compression system, an obvious preliminary experiment was to use the LPC optimal filter to predict the cavity shape from the measured cavity response. This technique had been reported as a means to compute vocal tract area functions from speech data so we felt that simple cylindrical cavities would be no problem for the optimal filter technique. The results of these tests were inscrutable as were the results of similar attempts made on speech data. We could not see the shape of simple cavities in the reconstructed area function derived from the optimal filter.

In order to resolve the above mentioned anomalies, we were led to experimentally investigate the use of the optimal filter as an area predictor. The optimal filter is, of course, at the heart of the LPC speech compression algorithm. It has been shown by other workers that if the vocal tract is modelled as a series of segments, each with constant cross section, then the optimal filter coefficients derived from speech data yield the cross sectional areas of the segments. This has been tested in the past on theoretical cavity data and on speech data. In this report we present the first application of the technique to actual cavity data derived from a cavity with a directly measureable area function.

There are several reasons for performing such a series of experiments. First, they provide the most direct test of the theoretical link between optimal filter coefficients and cavity segment area functions. It is necessary to establish confidence in this very physical interpretation of the optimal filter if one is to accept the vocal tract area functions derived thereby as having validity.

Another motivation for the present work was the feeling that if the

optimal filter does indeed represent an extraction of the vocal tract area function from the speech data, then a modification of the filter which makes it better represent the area function may have consequence in the speech compression applications of the filter. The work has not yet arrived at a point where this contention can be verified, but the experiments completed have indicated a length correction modification to the filter is necessary in order that it extract the actual area function from cavity data. The impact of this correction on compression of speech may be an interesting extension of the present work.

A third motivation for the experiments reported here is that the specifications of the vocal tract area function during articulation is a problem which has generated a great deal of work quite independent of the question of speech compression. The optimal filter then represents the intersection of these two independent and quite active speech research trajectories, and as such is obviously fertile ground for investigation.

The present study although preliminary in respect to the above mentioned questions has nevertheless yielded some quite interesting conclusions. The major accomplishments during the past quarter may be summarized briefly in the following list:

1. The impulse response of a collection of acoustical cavities has been measured. All of the cavities are constructed of uniform circular segments.
2. The cavity spectra as derived from the measured impulse response, has been fit fairly accurately by a model based on the lossless transmission line equations but with an extra inductive length correction added at each segment junction in the cavity.
3. The optimal filter technique has been used to derive the cavity area functions from the experimentally observed cavity spectra, as well as from the theoretically predicted spectra. These derived area functions are thenc ompared to the actual cavity.

From this work the following conclusions may be drawn:

1. The derived area functions are always longer than the original cavity.
2. The area functions derived from actual data always seem to be more difficult to interpret than those derived from theoretical spectra, even though the theoretical spectra fit the data quite well.
3. Step changes in the area function of the original cavity were always larger than the corresponding changes in the derived area function.

INTRODUCTION

Specification of the shape of the vocal tract during articulation is a problem which has motivated a great deal of research [1-7]. Wakita [7] has recently summarized the efforts of workers in this field. The most recent contributions have been based on optimal filtering, a technique utilized in speech compression work [8 -10]. The optimal filter is a filter which, when applied to a segment of speech data, reduces the data to white noise. Information in the speech data is then contained in the filter coefficients. If the vocal tract is modelled as a series of axially symmetric segments (cf, Figure 2.2), each segment having a constant cross sectional area, then the optimal filter coefficients may be transformed into cross sectional areas for the segments [6 , 7]. Thus the optimal filter derived from speech data yields a step-wise approximation to the vocal tract cross sectional area.

This paper describes an experimental study of the optimal filter technique for deducing area functions from acoustical cavity data. The cavities are all constructed of cylindrical segments of tubing, so the area function is a series of uniform steps. All measurements are made in the regime where only plane waves propagate in the cavities. The cavities are impulsed with a band limited (<5kHz) delta function and the impulse response is measured. This data is converted to an optimal filter from which the cavity area function is computed and compared to the known cavity area function.

A theory is presented from which spectra may be computed from area functions. This theory is based on the lossless transmission line model which is isomorphic to the optimal filter formulation. However, it is shown here that an inductive length correction is necessary at every cross section discontinuity in order to correctly predict the observed spectra. This length correction was originally worked out for a single step in cavity cross section [11]; in this work it is generalized to a cavity with an arbitrary number of steps.

In Chapter 1, the general theory for sound transmission in axially symmetric cavities is reviewed and reformulated. Chapter 2 deals with the theory of cavities comprised of segments of uniform cross section. The general length correction is derived and the optimal filter technique is reviewed. Several examples are given of spectra derived from area functions and area functions derived from spectra. Chapter 3 contains the results of experimental measurements on real cavities. Chapter 4 summarizes the work presented here.

CHAPTER 1. CYLINDRICAL CAVITIES-GENERAL THEORY

1.1 THREE DIMENSIONAL WAVE EQUATION

Consider a cavity with uniform cross section oriented along the z-axis, as shown in Figure 1.1. Sound transmission in such a cavity is described by the general wave equation.

$$\nabla^2 \Psi = \frac{1}{c^2} \frac{\partial^2}{\partial t^2} \Psi, \qquad 1.1$$

where Ψ is a scalar potential, c is the velocity of sound, and ∇^2 is the three-dimensional Laplacian operator. This equation is valid if the ambient gas is in the thermal equilibrium and if pressure fluctuations are small compared to ambient pressure and particle velocity fluctuations are small compared to c.

Wave equations for pressure and particle velocity may be derived by substitution of the following relationships into Equation 1.1:

$$p = \rho \frac{\partial \Psi}{\partial t}, \qquad 1.2$$

$$\vec{v} = - \vec{\nabla} \Psi ,$$

where p is pressure, v is particle velocity and ρ is the ambient gas density. It is convenient to separate out the time dependence of the solution of Equation 1.1 by assuming that the potential is of the form:

$$\Psi = \Psi (x,y,z) \, e^{-i\omega t}. \qquad 1.3$$

This separation yields the equation

$$(\nabla^2 + k^2) \, \Psi(x,y,z) = 0, \qquad 1.4$$
$$k^2 = (\omega/c)^2.$$

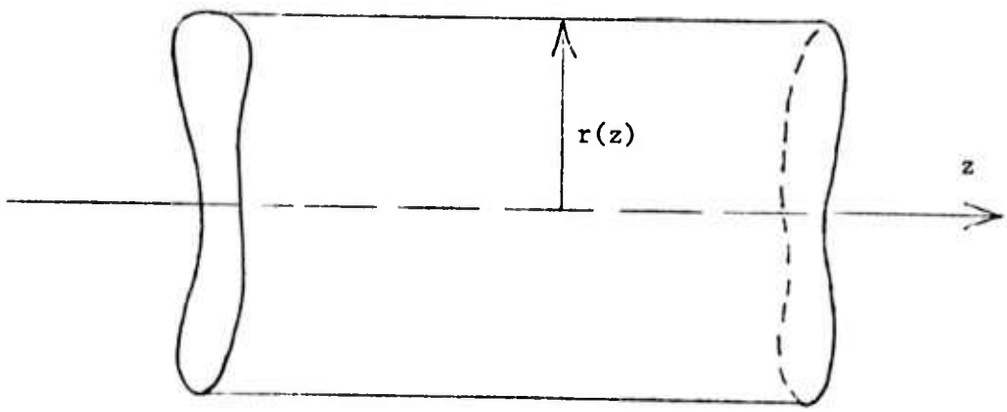

Figure 1.1 Uniform Cavity Oriented Along the z-axis

Now the symmetry of the cavity suggests a further separation of the spatial coordinates

$$\Psi(x,y,z) = \psi(x,y)e^{ik_z z}, \qquad 1.5$$

$$k^2 = k_z^2 + \kappa^2.$$

Putting Equation 1.5 back into Equation 1.4 gives the wave equation the form

$$(\nabla_2^2 + \kappa^2)\psi(x,y) = 0, \qquad 1.6$$

where ∇_2^2 is the two-dimensional Laplacian in x and y.

If the cavity wall is perfectly rigid, as will be assumed in this treatment, then the velocity normal to the wall at the wall must vanish. Using Equation 1.2, this boundary condition may be expressed

$$\vec{\nabla}_\perp \psi = 0, \qquad 1.7$$

Where $\vec{\nabla}_\perp$ is the gradient operator perpendicular to the wall evaluated at the wall.

The above equations specify an eigenvalue problem with a general solution of the form.

$$\Psi(x,y,z,t) = \sum_n A_n \psi_n(x,y) e^{ik_n z} e^{-i\omega t}. \qquad 1.8$$

$$k_z^2 = k_n^2 = k^2 - \kappa_n^2 = \frac{\omega^2}{c} - k_n^2,$$

where n is an index on the eigenstates.

From Equation 1.8 it is evident that the nth cavity mode will not propagate if k_n is imaginary. It can also be seen from Equation 1.8 that the n^{th} mode has a cutoff frequency determined by the relationship.

$$\omega_{c,n} = c\kappa_n \qquad 1.9$$

where $\omega_{c,n}$ is the cutoff frequency. At frequencies lower than $\omega_{c,n}$ the n^{th} mode is exponentially damped by the $\exp(ik_n z)$ term in Equation 1.8 and will not propagate. For a cavity with rigid walls, the fundamental mode (n=0) has $\kappa_o = 0$. This mode is a plane wave propagating with velocity c. As long as $\omega < \omega_{c,n}$, only plane waves propagate.

For the relatively simple case of a uniform cylindrical cavity of

radius b, the general expressions of Equation 1.8 take the form

$$\Psi(x,y,z,t) = \Sigma_{m,n} A_{m,n} \psi_{m,n}(r,\phi) e^{ik_n z} e^{-i\omega t}. \qquad 1.10$$

$$\psi_{mn}(r,\phi) = \begin{matrix}\cos \\ \sin\end{matrix} (m\phi) J_m(\kappa_{mn} r),$$

where r,ϕ are polar coordinates relative to the z axis, J_m is a Bessel function and m is an index on aximuthal modes. As seen earlier in the general case, the fundamental mode has $\kappa_{oo} = 0$ and propagates as a plane wave along the z-axis. The boundary condition at the cavity wall is expressed from Equation 1.7 as

$$\kappa_{mn} \nabla_r J_m(\kappa_{mn} r)\Big|_{r=b} = 0 \qquad 1.11$$

For the fundamental mode this condition is obviously met. For higher order modes, however, $\kappa_{mn} > 0$; for these modes to exist, κ_{mn} must be large enough to satisfy the equation.

$$\nabla_r J_m(\kappa_{mn} r)\Big|_{r=b} = 0. \qquad 1.12$$

The first mode above the fundamental turns out to be the $J_1(\kappa_{10} r)$ mode. The constraint expressed in Equation 1.12 when applied to this mode yields the condition

$$\nabla_r J_1(1.8413\cdots) = 0. \qquad 1.13$$

So the cutoff frequency for the first mode above the fundamental is

$$\omega_{c,10} = 1.8413 \frac{c}{b} \qquad 1.14$$

Notice here that as the radius, b, of the cavity grows larger, the cutoff frequency for higher modes decreases. Figure 1.2 is a plot of the log cutoff frequency of a uniform cylindrical cavity as a function of cavity radius. The first few modes are shown in this graph.

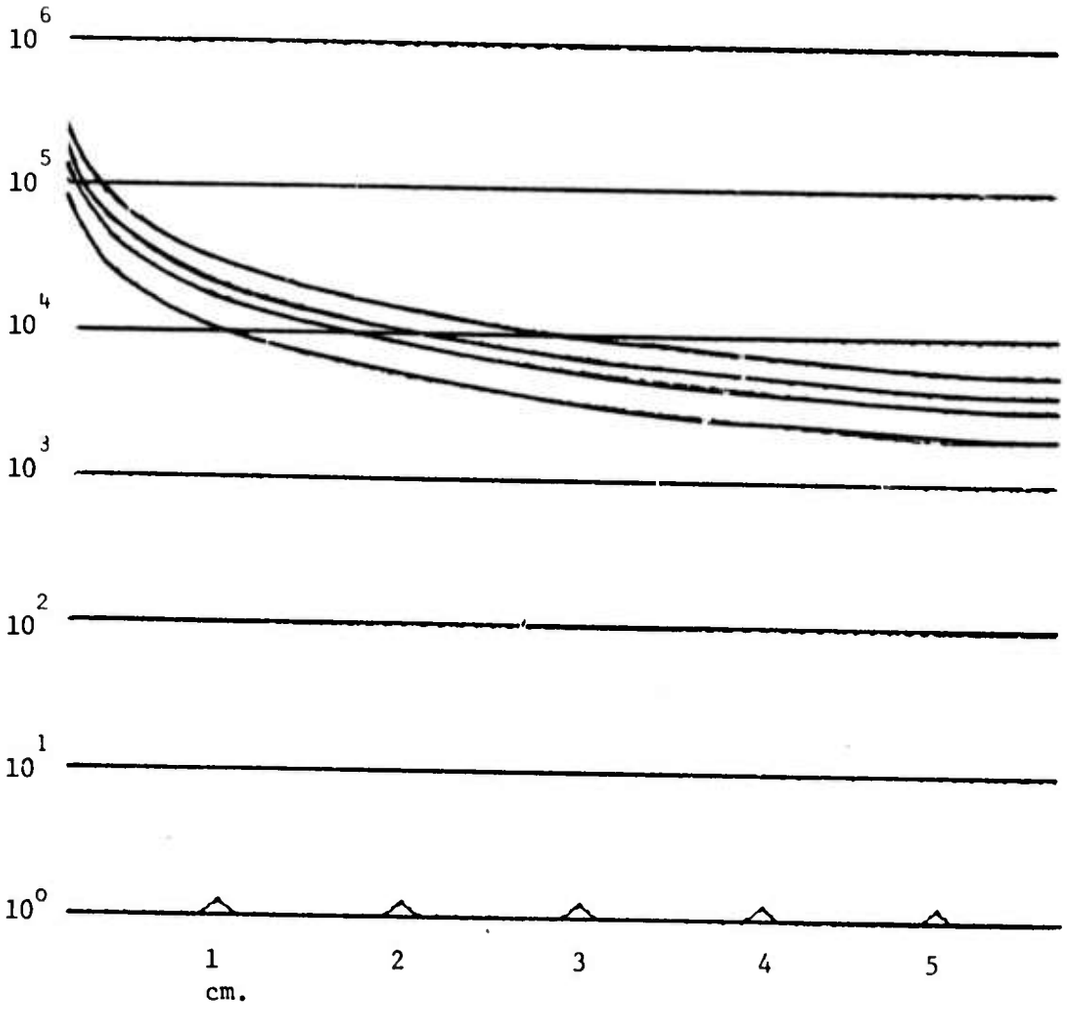

Figure 1.2 Log Cutoff Frequency vs Cavity Radius for the First Few Transverse Modes of a Uniform Cylindrical Cavity

1.2 WEBSTER'S EQUATION

The previous section dealt with cavities of uniform cross section. If this restriction is lifted, the eigenvalue problem becomes more difficult, as might be expected. However, if Equation 1.14 is satisfied for all values of b, where b now depends on z, and if the cross sectional area is slowly varying, then the general wave equation may be replaced with an approximate equation known as Webster's Equation [12]. The approximate equation has the form

$$\frac{\partial^2 \Phi}{\partial z^2} + \frac{1}{A(z)} \frac{\partial A(z)}{\partial z} \frac{\partial \Phi}{\partial z} = \frac{1}{c^2} \frac{\delta^2 \Phi}{\delta t^2} , \qquad 1.15$$

where A(z) is the cross sectional area and Φ is a scalar potential which depends only on z and t. By removing the time dependence as in the previous section (cf, Equations 1.3, 1.4), Equation 1.15 becomes

$$\frac{\partial^2 \Phi(z)}{\partial z^2} + \frac{1}{A(z)} \frac{\partial A(z)}{\partial z} \frac{\partial \Phi(z)}{\partial z} + k^2 (z) = 0, \qquad 1.16$$

$$k^2 = \frac{\omega^2}{c} .$$

Equations in pressure and velocity may be derived by combining Equation 1.2 and Equation 1.16.

For the case of a uniform cross section, Equation 1.16 reduces to the one-dimensional wave equation with plane wave solutions. Notice that since the wave equation is one-dimensional, transverse modes to not appear in this formulation. This is why its use is restricted to those cases which satisfy Equation 1.14. In the general case where A(z) is not constant, the solution of Equation 1.16 is not a plane wave, but a one-parameter wave [13], in that only z dependence is allowed. For example, a conical horn cross section yields a spherical wave solution in the z coordinate. The spherical wave is not plane, but it is completely specified by one coordinate.

1.3 UNIFORM CYLINDRICAL TUBES

The results of the previous section (specifically Equation 1.16 with A(z)=constant), may be used to derive the canonical solutions of the organ pipe problem. A uniform tube of length L, open at both ends has eigenfunctions.

$$\Phi(z,t) = B \cos \frac{n\pi z}{L} e^{-i\omega t}, \qquad 1.17$$

$$n = 0,1,2,\cdots .$$

The eigenfrequencies for this case are

$$f_n = \frac{nc}{2L}, \qquad 1.18$$

$$n = 0,1,2,\cdots .$$

For the same tube with one end closed and one open the eigenfunctions are

$$\Phi(z,t) = B \sin \frac{n\pi z}{2L} e^{-i\omega t}, \qquad 1.19$$

$$n = 0,1,2,\cdots .$$

and the eigenfrequencies are

$$f_n = \frac{nc}{4L} \qquad 1.20$$

$$n = 0,1,2,\cdots .$$

For a real tube the above results must be modified by an effective length correction. Plane wave inside of the tube must convert to spherical waves at an open end in order to radiate into space. This conversion causes an effective lengthening of the tube which may be written [13]

$$L_e \cong L + 0.4\sqrt{A} \qquad 1.21$$

where A is the area of the open end of the tube and L_e is the effective length of the tube. This effect will be discussed in greater detail in Chapter 2.

2.1 UNIFORM STEP APPROXIMATION

In Chapter 1, the Webster equation was introduced in order to deal with a cavity of varying cross section. Another approach to this problem is to approximate the varying cross section by a series of steps, each with constant radius. This is illustrated in Figure 2.1. This approach has been taken in the past and is sometimes referred to as the transmission line model [1 - 6]. As with the Webster equation approximation, the uniform step approximation will not yield information about higher order propagating modes. For this reason the cavity of interest must satisfy the cutoff criterion of Equation 1.14 in order that the step approximation give meaningful results. It also should be noticed that this is a more crude approximation than the Webster equation. To illustrate this fact, consider the conical horn. The Webster equation gives a spherical wave solution in the horn. The step approximation gives a plane wave in each segment, as will be shown below. Clearly the Webster equation solution is closer to reality.

Consider the case illustrated in Figure 2.2. Each of the N steps in this cavity has constant cross section. For convenience of computation, each end is terminated in an infinite length tube of uniform cross section. If all of the segments and the terminating tubes satisfy Equation 1.14, then the only propagating mode is the plane wave. Equation 1.16 reduces to the one-dimensional wave equation in each of the uniform segments. The wave equation solution in the n^{th} segment may be written

$$\Phi_n(z) = b_n^+(z)e^{ikz} + b_n^-(z)e^{-ikz} \qquad 2.1$$

where $b_n^+(b_n^-)$ is the complex amplitude of the wave traveling to the right (left) in the n^{th} section and the time dependence of Φ has been suppressed. Now, by introducing the vector notation

$$B_n = \frac{b_n^+}{b_n^-}, \qquad 2.2$$

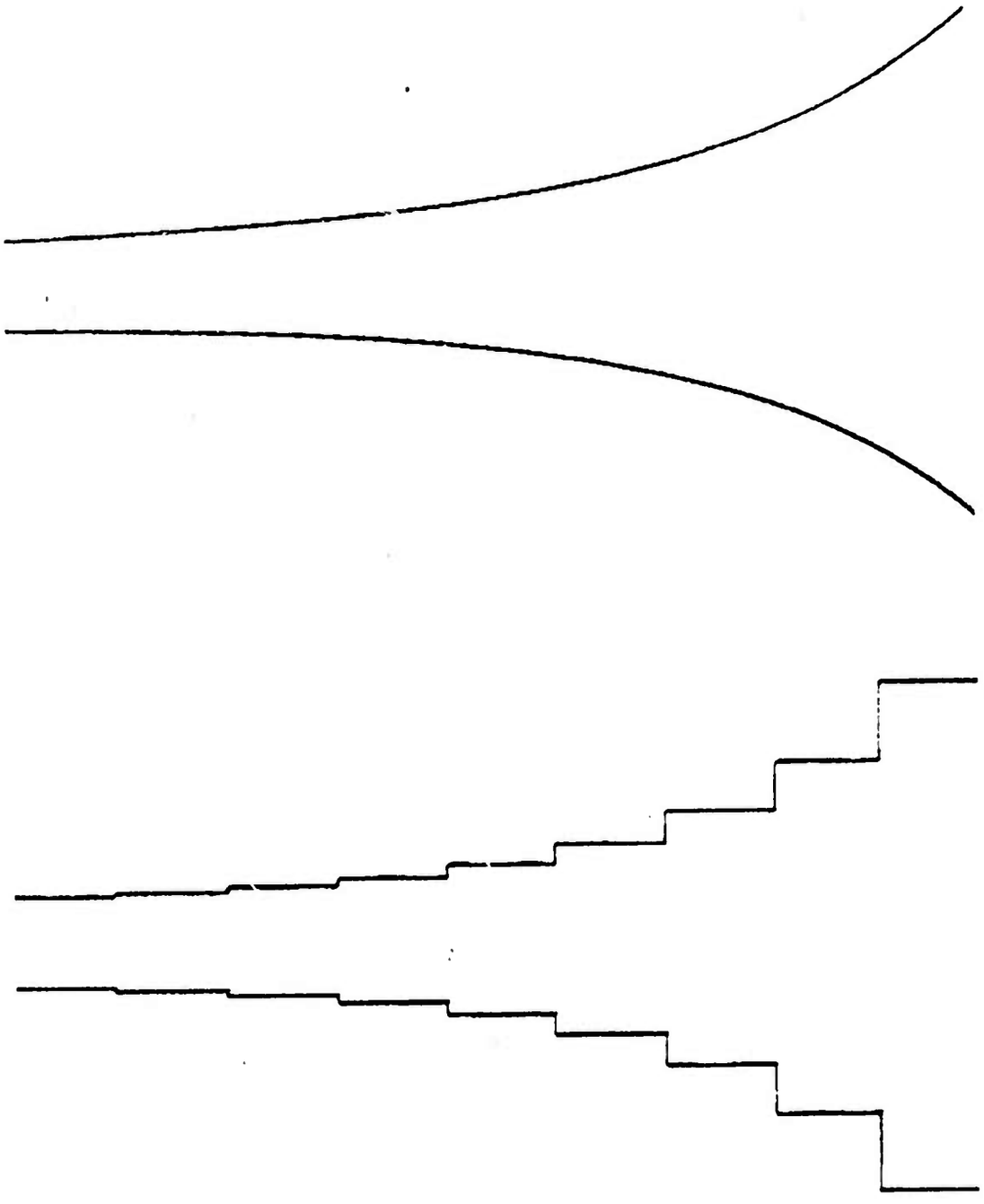

Figure 2.1 Uniform Step Approximation to a Cavity of Varying Cross Section

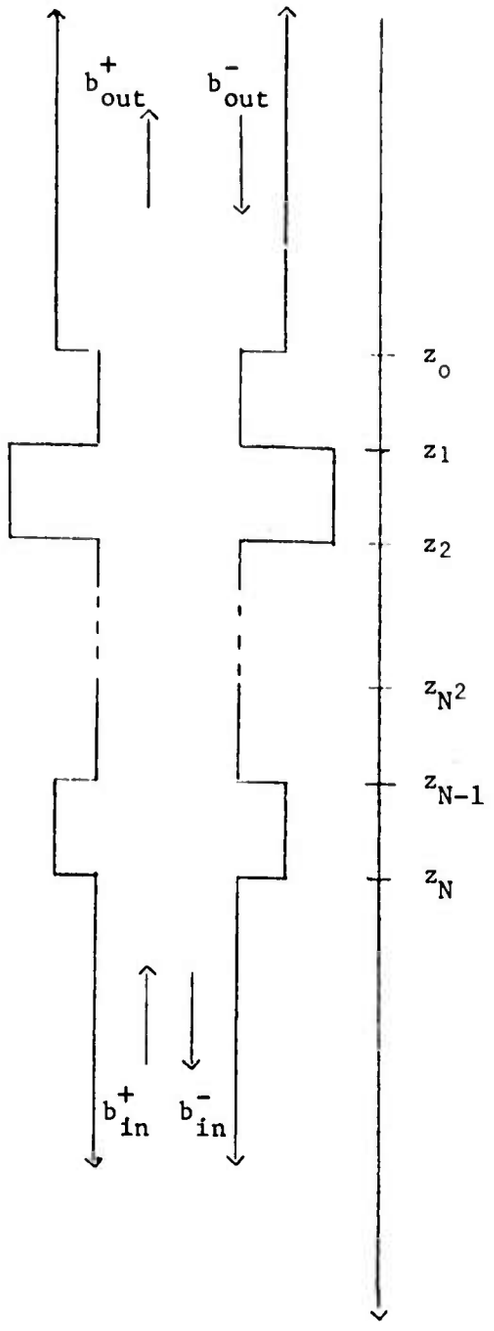

Figure 2.2 Sound Transmission in a Stepped Cavity

the propagation from z=0 to z may be represented by the propagator matrix T^{-1}. Defining this operation as an inverse matrix is a notational and computational convenience. The propagation is then expressed

$$B(0) = T\,B(z), \tag{2.3}$$

$$T = \begin{vmatrix} e^{-ikz} & 0 \\ 0 & e^{ikz} \end{vmatrix}$$

The foregoing discussion dealt with one uniform section of the tube shown in Figure 2.2. Now consider the junction of two adjacent sections. For conservation of mass and momentum, the pressure and volume velocity must be continuous across th junction. The volume velocity is just the particle velocity multiplied by the cross sectional area. By substituting Equation 2.1 into Equation 1.2, the pressure and volume velocity are found to be

$$p(z) = -i\omega\rho[b^{+}e^{ikz} + b^{-}e^{-ikz}], \tag{2.4}$$

$$A(z)v(z)\equiv u(z)=ikA(z)\ [-b^{+}e^{ikz} + b^{-}e^{-ikz}],$$

where u(z) is the volume velocity at z. Notice that p and u have components in both directions. Now the continuity of p and u across the junction between section n and section n+1 is expressed

$$b_n^{+} + b_n^{-} = b_{n+1}^{+} + b_{n+1}^{-}, \tag{2.5}$$

$$A_n(b_n^{+} - b_n^{-}) = A_{n+1}(b_{n+1}^{+} - b_{n+1}^{-}),$$

where A_n is the cross sectional area of section n. In the vector notation,

$$B_n(z) = R_n B_{n+1}(z), \tag{2.6}$$

$$R_n = \frac{1}{1+K_{n,n+1}} \begin{matrix} 1 & K_{n,n+1} \end{matrix},$$

$$K_{n,n+1} = \frac{A_n - A_{n+1}}{A_n + A_{n+1}}.$$

Here R_n is the reflection matrix representing the junction between section n and section n+1, $K_{n,n+1}$ is the reflection coefficient for this junction, and the B vectors are both evaluated at z_n, the position of

the junction.

Now by combining the propagation matrix, T for each segment and the R matrix for each junction, it is possible to write down the sound transmission equation for the cavity in Figure 2.2. In the vector notation:

$$B_{in} = R_N T_{N-1} R_{N-1} T_{N-2} \cdots R_1 T_1 R_0 B_{out}, \qquad 2.4$$

$$B_{in} = R_N \prod_{n=0}^{N-1} T_n R_n B_{out},$$

$$T_n = \begin{vmatrix} e^{-ik\ell_n} & 0 \\ 0 & e^{ik\ell_n} \end{vmatrix}.$$

Notice that T_n propagates the solution across segment n, where ℓ_n is the length of the segment. Since the cavity is terminated in infinite length tubes, no reflection occurs at the output, so $b^-_{out} = 0$. This fact allows the expression

$$B_{in} = b^+_{out} \left[R_N \prod_{n=0}^{N-1} T_n R_n \begin{pmatrix} 1 \\ 0 \end{pmatrix}\right] \equiv b^+_{out} D, \qquad 2.5$$

where D is the vector result of the matrix multiplications on the (1,o) vector.

Equation 2.5 is an expression for the output wave amplitude, B_{out}, in terms of the input wave, B_{in}. The squared gain function of the cavity may now be written

$$\left|\frac{b^+_{out}}{b^+_{in}}\right|^2 = \left|\frac{1}{d^+}\right|^2 \qquad 2.6$$

where d^+ is the top compnent of D. It can be shown [13] that the energy density of a propagating wave is

$$E(z) = \frac{1}{\rho c^2}\left[\left(\frac{\rho c}{A(z)}\right)^2 u^2(z) + p^2(z)\right], \qquad 2.7$$

where u is the volume velocity and p the pressure. Combining Equations 2.7, 2.4, and 2.5 allows the conservation of energy equation to be written

$$\left|b^+_{in}\right|^2 + \left|b^-_{in}\right|^2 = \left|b^+_{out}\right|^2, \qquad 2.8$$

or $|D|^2 = 1.$

The transmission spectrum of an arbitrary cavity of the form shown in Figure 2.2 may now be derived by use of Equations 2.5 and 2.6. First the T and R matrices are calculated from the cavity step lengths, ℓ_n, and the cross sectional areas, A_n. The D vector of Equation 2.5 is then calculated by the product of all of the matrices acting on the (1,0) vector. The inverse square modulus of the d^+ component of the D vector is then calculated. This is the squared transmission spectrum as indicated in Equation 2.6.

The above formulation is equivalent to the transmission line model referred to in papers on optiomal filtering [6,7]. It can also be shown that the matrix operator of Equation 2.4 is isomorphic to an optimal inverse filter deriveable from the cavity signal [7]. The condition for this isomorphism is that the step length in the cavity be constant and related to the signal sample frequency by the expression

$$\frac{2\ell}{c} = \frac{N}{f_s} , \qquad 2.9$$

where ℓ is the step length, N the number of steps and f_s the sample frequency. Notice that all steps have the same length.

2.2 END CORRECTIONS

In section 1.2, and ad hoc length correction was introduced to account for radiation loading effects at the open end of a tube. In this section, a more concise treatment of the problem is presented.

As motivation for what is to follow, consider the case of a uniform tube of length L. For convenience, the tube is terminated on both ends with infinite length tubes. The transmission spectrum for this system may be calculated from the theory of section 2.0. Figure 2.3 shows the cavity with termination and the experimentally measured spectrum. Below the measured spectrum are three calculated spectra. The first is from Equation 2.4 with a tube length of L assumed. The second also uses Equation 2.4, but assumes a tube length of $L+.8\sqrt{A}$ where A is the cross sectional area of the tube. The third spectrum is calculated from the theory to be developed in this section.

If the tube and termination radii of the system in Figure 2.3 are within the limits of Equation 1.21, then only plane waves propagate. However, at the junction of the tube and the termination there is a radial surface with a boundary condition which cannct be fit with plane waves. This surface is the crux of the end correction problem.

There are three relevant length scales in this problem: the wave length of the sound radiation λ, the radius of the tube, r_1, and the radius of the termination tubes, r_2. If the termination tubes are not present, the tube is unflanged and the radiated sound must wrap around and fit boundary conditions on the outside of the tube. In this case, the radiated sound is not plane waves. Levine and Schwinger [14] have solved the semi-infinite unflanged tube in the frequency range where only plane waves propagate inside of the tube. A frequency dependent length correction is derived which has a value $.346\sqrt{A}$ at low frequencies. At higher frequencies, the correction becomes less. At $kr_1 = 1.841$, the cutoff limit for higher modes, the correction is down to $.254\sqrt{A}$. This result is to be compared with the correction of Equation 1.21, which is $.4\sqrt{A}$ for each end of an open tube. As is obvious, the unflanged tube correction is lower for all frequencies.

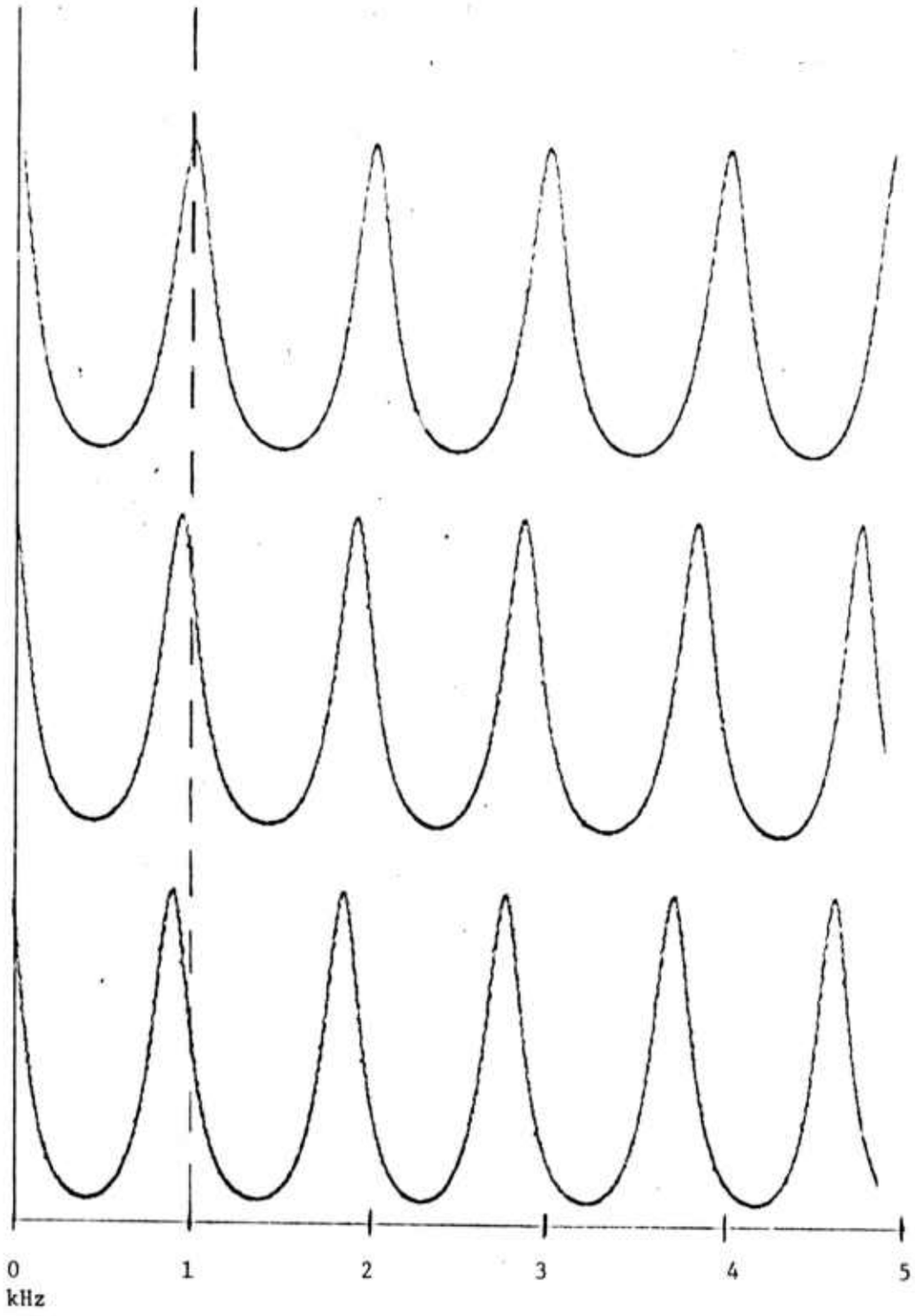

Figure 2.3 Uniform Tube with Termination
a. Spectrum; No Length Correction
b. Spectrum; $.8\sqrt{A}$ Length Correction
c. Spectrum; Theory of Section 2.2

If the termination tubes are present as in Figure 2.3, but have radii which are very large compared to the sound wavelength ($kr_2>>1$), then the tube is flanged. In this case, high order modes propagate in the terminating tubes, and these non-plane wave modes can fit the boundary condition (Equation 1.7) on the flange. This case is dealt with by Morse [13]. For $kr_2>1.5$, the length correction is $.479\sqrt{A}$ for each open end. This value is larger than the correction in Equation 1.21.

It is clear at this point that the ad hoc length correction for a uniform tube is between the actual length corrections for the flanged and unflanged tubes. The actual length correction depends not only on the tube area, but on the wavelength of the radiation and the size of the flange. Karal [11] has solved the case of a step discontinuity in a cylindrical tube where both sections are small enough that only plane waves propagate. The treatment satisfies the boundary condition at the tube discontinuity by treating the non-propagating modes locally. In the transmission line analogy, this is an inductive correction. The correction is $.479H\alpha$ where $H(\alpha)$ is a numerically calculated function with amplitude between zero and one; α is the ratio of tube radii at the discontinuity. This calculation will now be generalized to yield a length correction for a tube of N sections. The matrix approach will be used in order that the results may be combined with Equation 2.4 to yield a more accurate spectrum for a stepped tube.

First, consider the case of a single step discontinuity. The cavity is shown in Figure 2.4. It can be shown [11] that the volume velocity, $u(z)$ is continuous across the discontinuity, while the pressure is not. This may be expressed

$$p_1(0) - p_2(0) = u(0)Z_\alpha \qquad 2.10$$

$$u_1(0) = u_2(0) = u(0),$$

$$\alpha = \frac{r_1}{r_2} \quad ,$$

where the pressure discontinuity is represented as a lumped impedance at the change of cross section. Karal has treated the case where plane waves propagate in both directions in region 1, but only to the right in

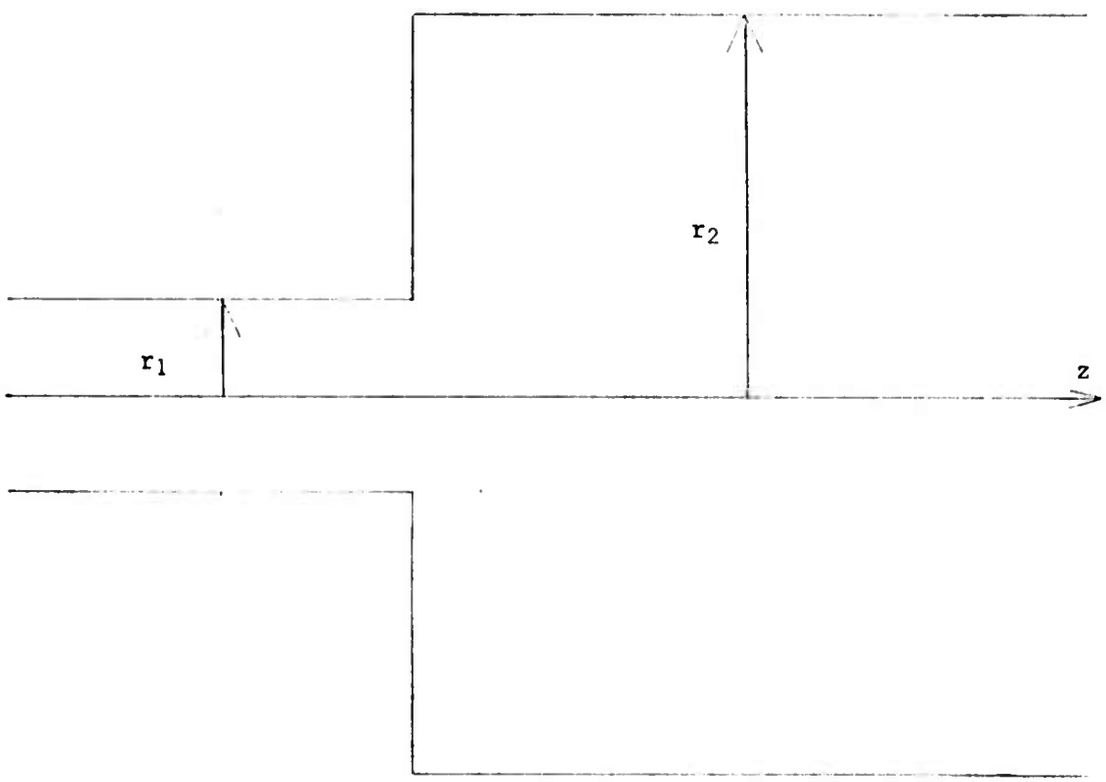

Region 1 Region 2

Figure 2.4 Tube with Step Continuity in Cross Sectional Area

region 2. In order to generalize to a cavity with more than one step, it will be assumed that plane waves propagate in both directions on both sides of the step. Using the notation developed in section 2.1, Equation 2.10 may be rewritten

$$(b_1^+ + b_1^-) - (b_2^+ + b_2^-) = \frac{iu(0)Z_\alpha}{\omega\rho} \qquad 2.11$$

$$u(0) = -ikA_1(b_1^+ - b_1^-) = -ikA_1(b_2^+ - b_2^-).$$

Combining these two results gives

$$b^+ + b^+ = \frac{(1 + kA_1Z_\alpha)b^+}{\omega\rho} + \frac{(1 - kA_1Z_\alpha)b^-}{\omega\rho}, \qquad 2.12$$

$$b_1^+ - b_1^- = b_2^+ - b_2^- .$$

Or, in vector notation,

$$B_1 = L\,B_2 , \qquad 2.13$$

$$L = \begin{vmatrix} 1 + \Theta & -\Theta \\ \Theta & 1 - \Theta \end{vmatrix},$$

$$\Theta = \frac{kA_1Z_\alpha}{2\omega\rho}, \quad B_1 = \begin{pmatrix} b_1^+ \\ b_1^- \end{pmatrix}, \quad B_2 = \begin{pmatrix} b_2^+ \\ b_2^- \end{pmatrix}.$$

Notice that by choosing A_1 as the cross sectional area in Equation 2.12, the lumped impedance has been placed in the smaller tube. From Karal [11],

$$Z_\alpha = i\omega \frac{8\rho}{3\pi^2 r_1} H_\alpha, \qquad 2.14$$

where H_α is computed numerically and shown in Figure 2.5. It is seen that Z_α has the form of a inductive impedance. Now putting Equation 2.15 back into 2.13 gives

$$\Theta = -\frac{i4}{\pi} kr_1 H_\alpha \qquad 2.15$$

$$k = \omega/c.$$

At this point, it is possible to write a transfer function for the N-step cavity of Figure 2.2 which includes length corrections for each step. Combining Equations 2.4 and 2.13 gives

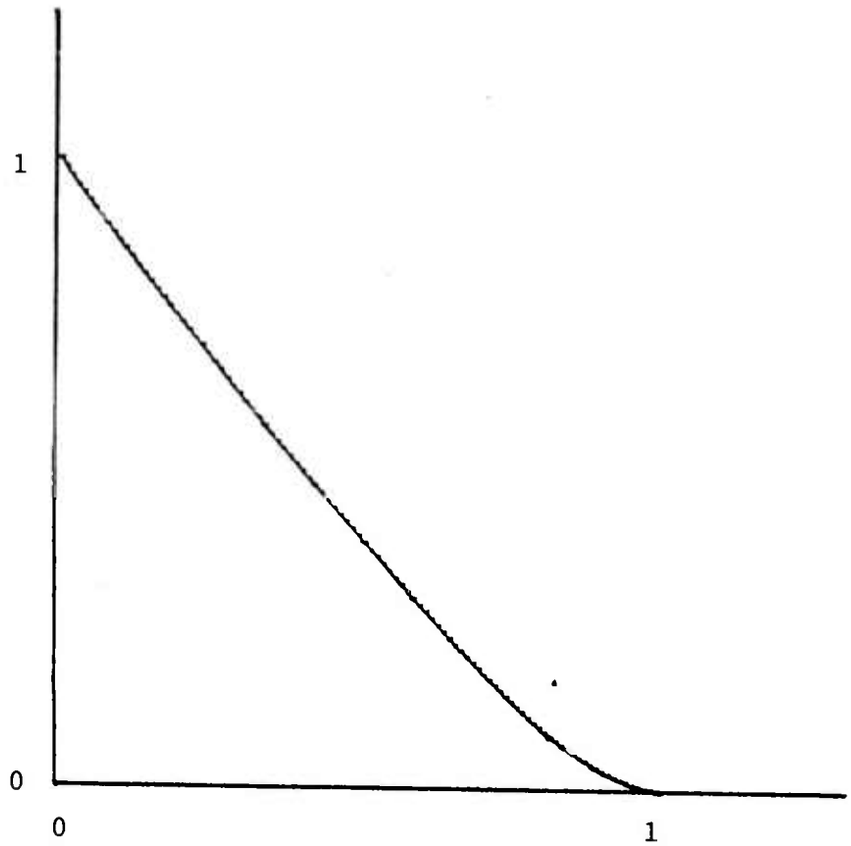

Figure 2.5 Plot of Length Correction Function H_α vs α

$$B_{in} = R_N L_N \prod_{n=0}^{N-1} T_n R_n L_n B_{out} \qquad 2.16$$

$$= \underbrace{L_N R_N}_{r_n < r_{n-1}} \prod_{n=0}^{N-1} T_n \underbrace{L_n R_n}_{r_n > r_{n+1}} B_{out}.$$

The brackets indicated that the sequencing of the R and L matrices depends on the ratio of radii at a given junction. The L correction always falls on the side with the smaller radius.

The transfer function of Equation 2.16 has been calculated for several different cavity shapes. Appendix 1 contains a flow chart for the coding; the next section describes the results of these calculations.

2.3 CAVITY SPECTRA DERIVED FROM AREA FUNCTIONS

This section contains several examples of spectra derived from area functions. The computation is based on the theory developed in the preceding sections; a flow chart for the coding of the problem appears in Appendix 1. The spectra which are referred to as uncorrected are computed from Equations 2.5 and 2.6; these spectra have no length correction. The spectra referred to as corrected have a length correction and are computed from Equation 2.16. Both cases are contained in the flow chart in Appendix 1. The general effect of the length correction is to shift the spectral peaks to downward in frequency, corresponding to a lengthening of the cavity.

Figure 2.6 is a plot of log spectra from 0 to 5kHz of a uniform tube of length 17 cm. with different radii. The top set of spectra (2.6a) is uncorrected; the bottom set is corrected. In both sets, the tube radius increases from bottom to top, taking values of .468, .775, 1.0, 1.295, and 1.5 cm. The tubes are all terminated in infinite length uniform tubes of radius 1.85 cm. to prevent reflections at the ends. In both sets of spectra the resonances are more sharply defined for the smaller tube radii. This is because the end reflection coefficients increase as the ratio of tube radius to termination radius decreases. This enhances the resonances. For the uncorrected spectra, the position of the spectral peaks does not vary with tube radius. However, in the corrected spectra, the peaks first decrease in frequency as the radius increases, then they increase as the radius continues to increase. This effect is more noticeable at higher frequencies. The source of this variation of resonant frequency with tube diameter is seen in Equations 2.13, 2.14, and 2.15. The strength of the length correction is determined by the parameter Θ in Equation 2.13. If $\Theta = 0$, the length correction matrix reduces to the identity matrix. As Θ deviates from zero the length correction increases. As can be seen in Equation 2.15,

$$\Theta \propto fr_1 H_\alpha,$$

a)

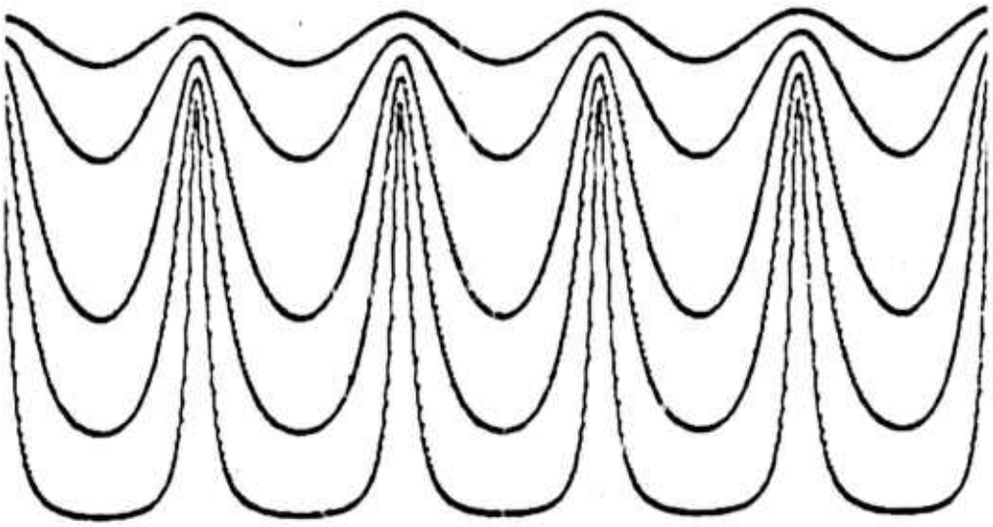

b)

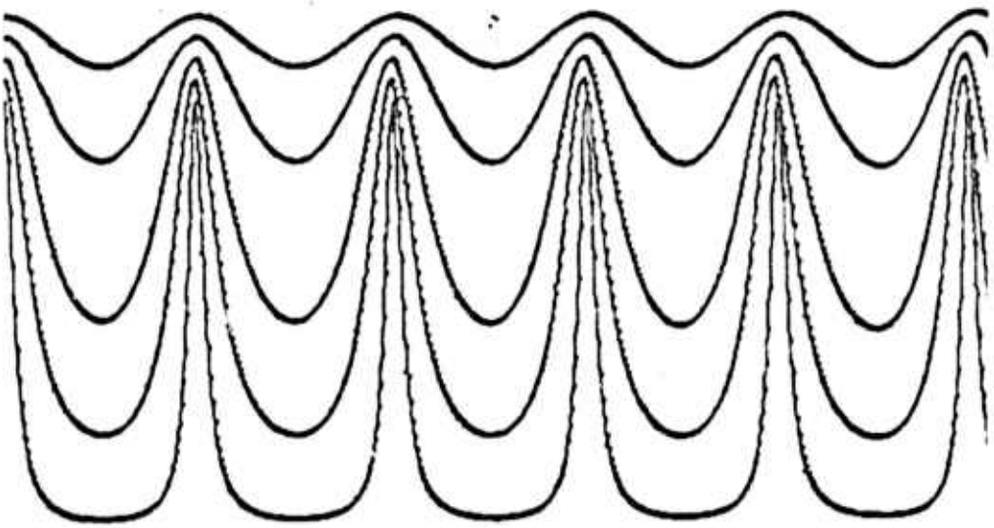

Figure 2.6 Uniform Tube Log Spectra From 0 to 5kHz with Varying Termination Radius
a. Uncorrected
b. Corrected

where r_1 is the tube radius, f is frequency, and H_α is given in Figure 2.5. As r_1 increases, H_α goes to zero, therefore, this function has a maximum at which point the length correction is largest. The f factor causes the peak to be more enhanced at higher frequencies. This explains the spectra in Figure 2.6b.

Figure 2.7 is a set of corrected log spectra from 0 to 2.5kHz for a uniform tube of length 17 cm. and radius .468 cm. The termination radius decreases from 2.0 cm. (bottom spectrum) to .5 cm. (top spectrum). As the termination radius increases, the resonant peaks shift to higher frequency. This is expected from Equation 2.16.

Figure 2.8 shows two sets of log spectra from 0 to $5kH_z$ for tubes of fixed radius (.468 cm.) with varying length. The length takes values 15,16,17,18,19 cm. As the length increases, the resonant peaks move lower in frequency. The top set of spectra is uncorrected, the bottom set is corrected. The corrected spectra have peaks which are lower in frequency, a result of the effective increase in length.

Figure 2.9 shows log spectra from 0 to $5kH_z$ for a stepped tube configuration. The cavity is shown in Figure 2.13. The termination radii are both 2.0 cm. The cavity steps have radii .7, 1.5, .7 cm. and respective lengths of 5.1, 6.8, 5.1 cm., for a total length of 17 cm. The bottom spectrum is corrected, so the peaks appear shifted to lower frequencies.

Figure 2.10 shows three sets of log spectra from 0 to $5kH_z$. The cavity in this case is a uniform tube 17 cm. long with radius 1.0 cm. The termination tubes have radii 2.0 cm. In the top spectra (2.10a) an aperture of length 0.1 cm. and variable radius is inserted at the input end of the 17 cm. tube. The top spectrum has the aperture radius equal to the tube radius and the peaks are those of a tube of length 17.1 cm. As the aperture radius closes down from 1.0 to 0.1 in steps of 0.1, the peaks shift downward in frequency and approach the resonance values of a tube closed at one end (cf., Equation 1.20). The high frequency peaks become attenuated by the presence aperture, which is short (0.1 cm.) and therefore has a very broad resonance at 0Hz which multiplies the line structure of the longer tube.

In Figure 2.10b an aperture is inserted on both ends of the long tube.

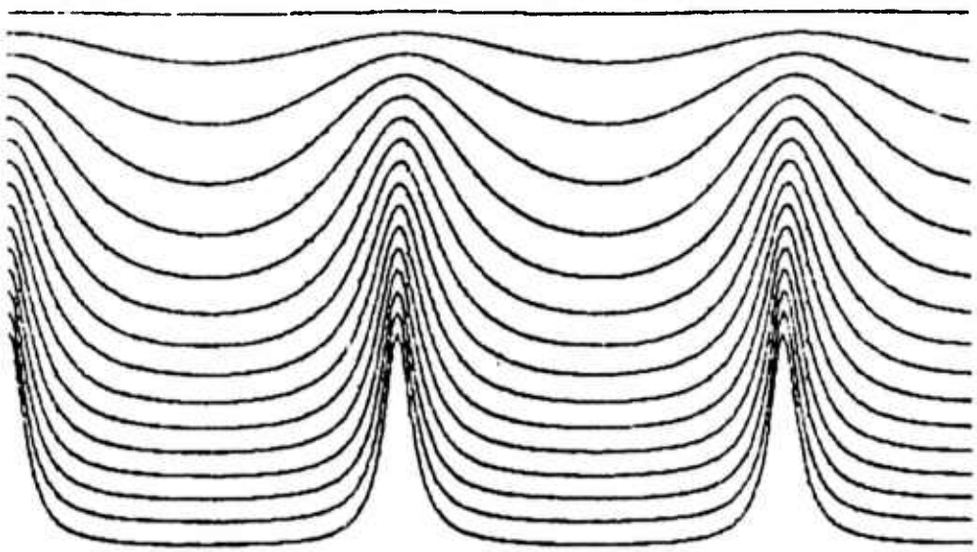

Figure 2.7 Uniform Tube Log Spectra From 0 to 2.5kHz with Fixed Termination and Varying Radius

a)

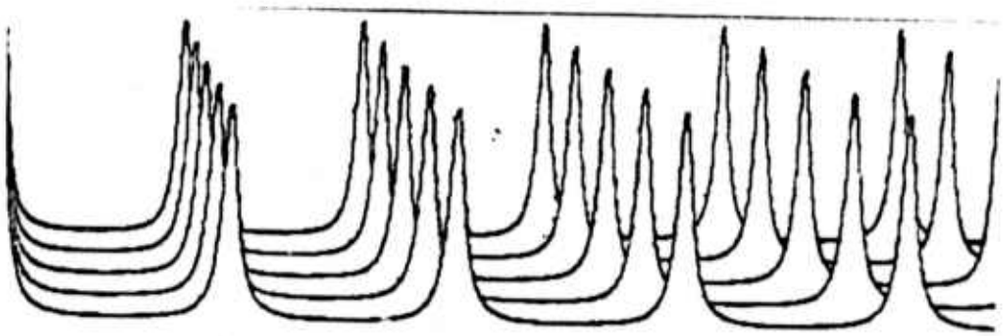

b)

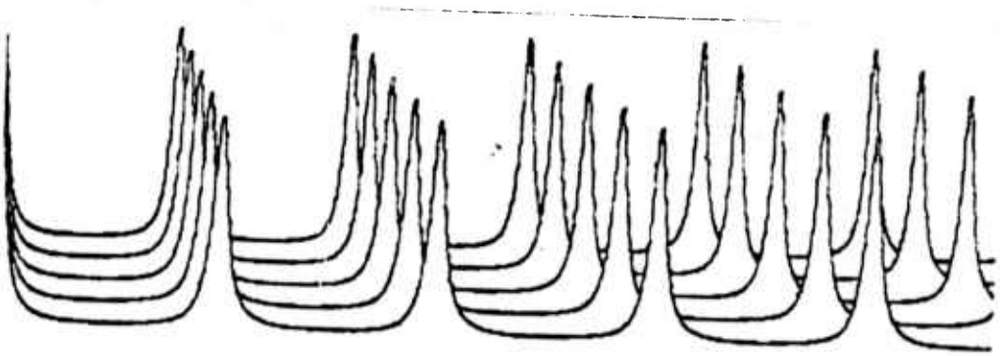

Figure 2.8 Uniform Tube Log Spectra From 0 to 5kHz with Fixed Termination and Radius and Varying Length
a. Uncorrected
b. Corrected

a)

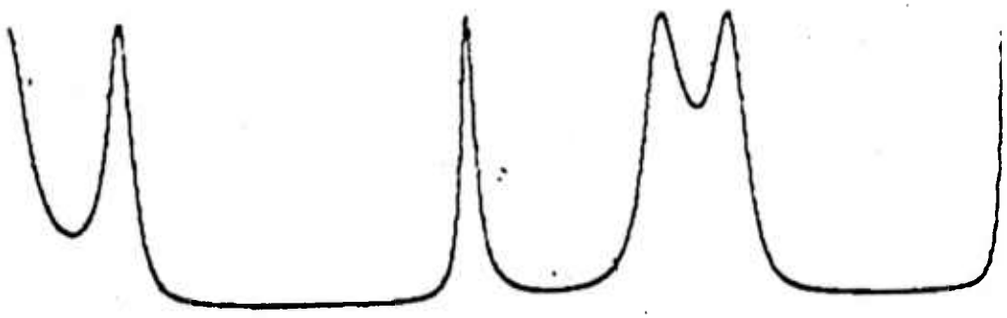

b)

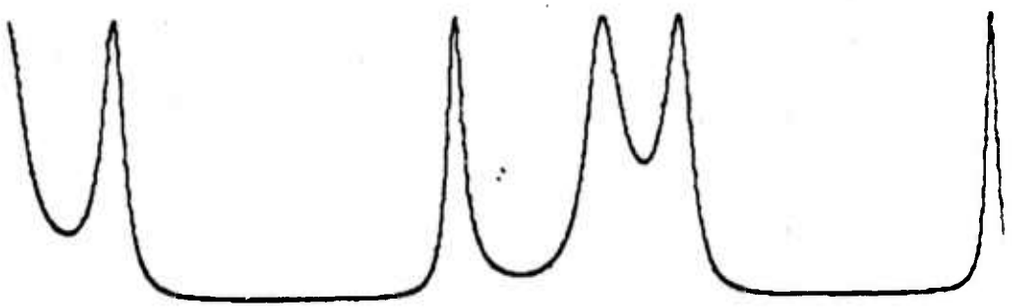

Figure 2.9 Log Spectra From 0 to 5kHz for a 3 Segment Cavity (Cavity Shown in Figure 2.13)
a. Uncorrected
b. Corrected

a)

b)

c)

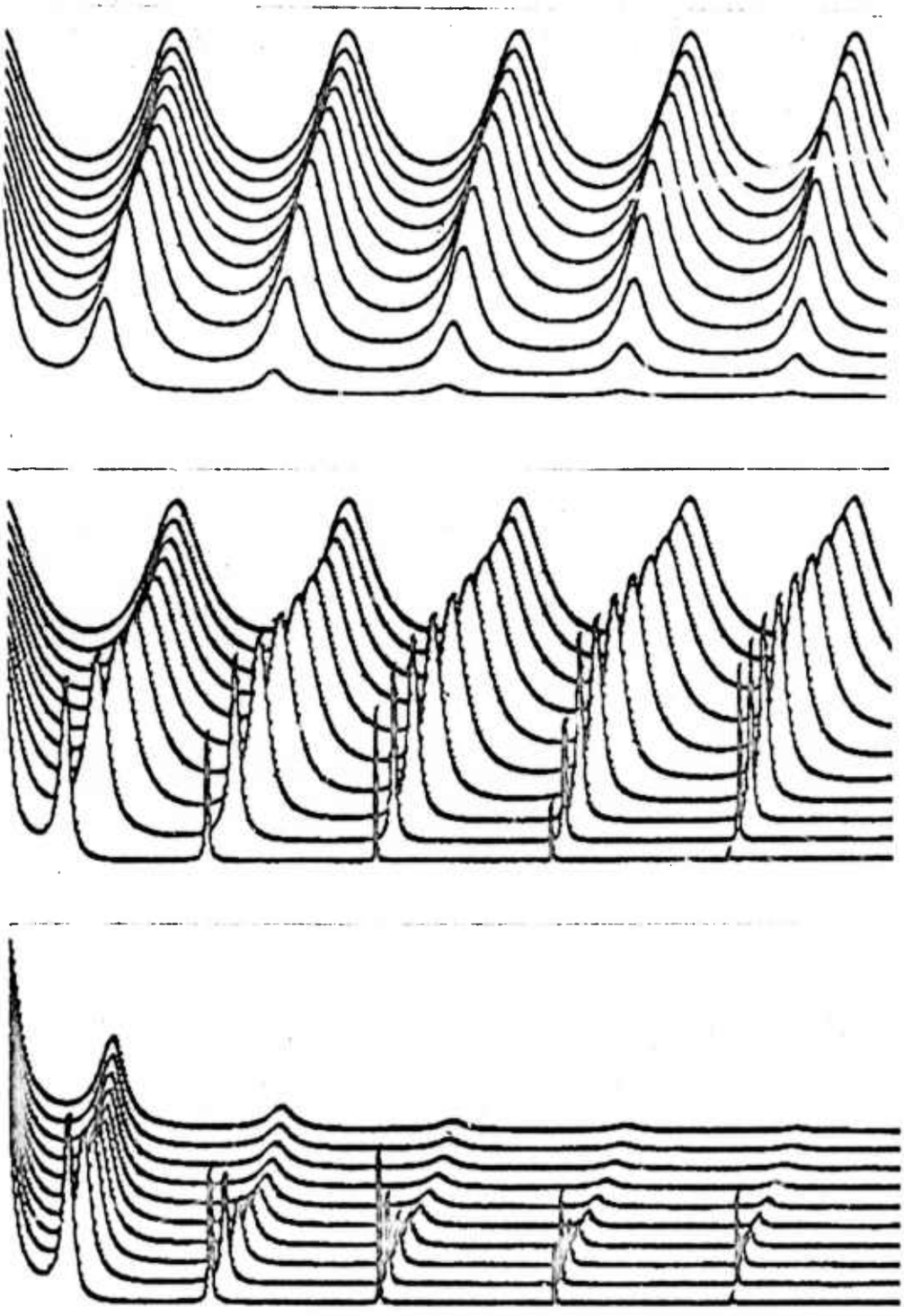

Figure 2.10 Corrected Log Spectra From 0 to 5kHz for a Uniform Tube with Apertures of Varying Radius on the Ends

a. Aperture Stopping Down on Input
b. Aperture Stopping Down on Both Ends
c. Aperture Down on Input; Stopping Down on Output

As the two apertures stop down the spectral peaks decrease, each one approaching the original position of the one just below it in frequency. This occurs because a tube open at both ends has the same spectrum as a tube closed at both ends. The effect of the aperture spectra is seen in the modulation of the peak amplitudes for small aperture radii.

2.4 CAVITY AREA FUNCTIONS DERIVED FROM SPECTRA

The previous section dealt with the deviation of spectra from area functions, a fairly straight forward calculation based on results derived earlier in this chapter. This section treats the inverse problem by the optimal filter technique. The detailed theoretical development of this approach has been published by others [6, 7] and will only be briefly outlined here.

Given a discretely sampled signal, S_j, the ith autocorrelation coefficient, Ri, is defined

$$Ri = \sum_{j=0}^{N-1} S_j S_j + |i|. \qquad 2.17$$

The filter coefficients, a_j, for the optimal filter are derived from the signal autocorrelation coefficients by solving the set of normal equations

$$\sum_{j=1}^{M} A_j R_{|i-j|} = -R_i, \quad i=1, \cdots, M. \qquad 2.18$$

The set of equations are solved recursively by the method of Levinson. The cavity reflection coefficients, Ki, are derived directly from the a_j [7]. But the reflection coefficients are related to the area, A_i, the cavity segments by the expression

$$K_i = \frac{A_i - A_{i+1}}{A_i + A_{i+1}}, \qquad 2.19$$

therefore, the cavity area function is derived from the Ki's, modulo a constant scale factor. The length scale follows from the sample frequency, f_s, and the speed of sound, c, by the relationship [6]

$$\ell = \frac{cfs}{2}, \qquad 2.20$$

where ℓ is the length of one segment of constant cross section. Notice all segments have the same length in this case, whereas in computing the spectra of general cavities (Equation 2.16) this constraint is not necessary.

This basic scheme has been implemented and applied to several theoretical cavity spectra. The approach is to specify a hypothetical cavity area function, compute uncorrected and corrected spectrum from the theory of this chapter and compute the area function from the spectrum. The results of several test cases are described below. The step length in all

of the examples is 1.7 cm., derived from Equation 2.20 for a Nyquist frequency of 5kHz.

Figure 2.11 illustrates the case of uniform tubes of fixed radius and lengths 15, 16, 17, 18, and 19 cm. The step in the area function is at the tube mouth where the output termination tube connects. The original tubes are shown on the overlays. Figure 2.11b shows the area functions computed from the uncorrected tube spectra. Notice that the fit is excellent for 17 cm., a case where the segment length 1.7 is integrally related to the cavity length. When this is not the case, the fit is not so perfect. In all cases, the step in the reconstructed area function is smaller than the original step. Figure 2.11c shows area functions derived from the corrected theoretical tube spectra. As will be seen later, these spectra are very close to the actual measured tube spectra, so this case is more relevant to the problem of real data. Notice that the derived tube is longer than the original as a result of the length correction.

Figure 2.12 is also a case of uniform tubes but in this case the lengths are all multiples of the step length, 1.7 cm. The tube lengths are 13.6, 15.3, 17, 19.7 and 21.4 cm. Notice how perfect the fit is for the area function derived from the uncorrected spectrum (Figure 2.12b). However, in the more relevant case of the corrected spectra (Figure 2.12c), the fit is not so good and the lengthening of the derived area function is again observed. Figure 2.13 shows the case of a terminated cavity with three segments. The area function derived from the uncorrected spectrum is once again very good. But the area function derived from the corrected spectrum, which is close to the measured spectrum, is not so good. Here one begins to see the problem of interpreting these derived area functions. Note that the error in length of the derived cavity has now distributed itself over the segments in some manner.

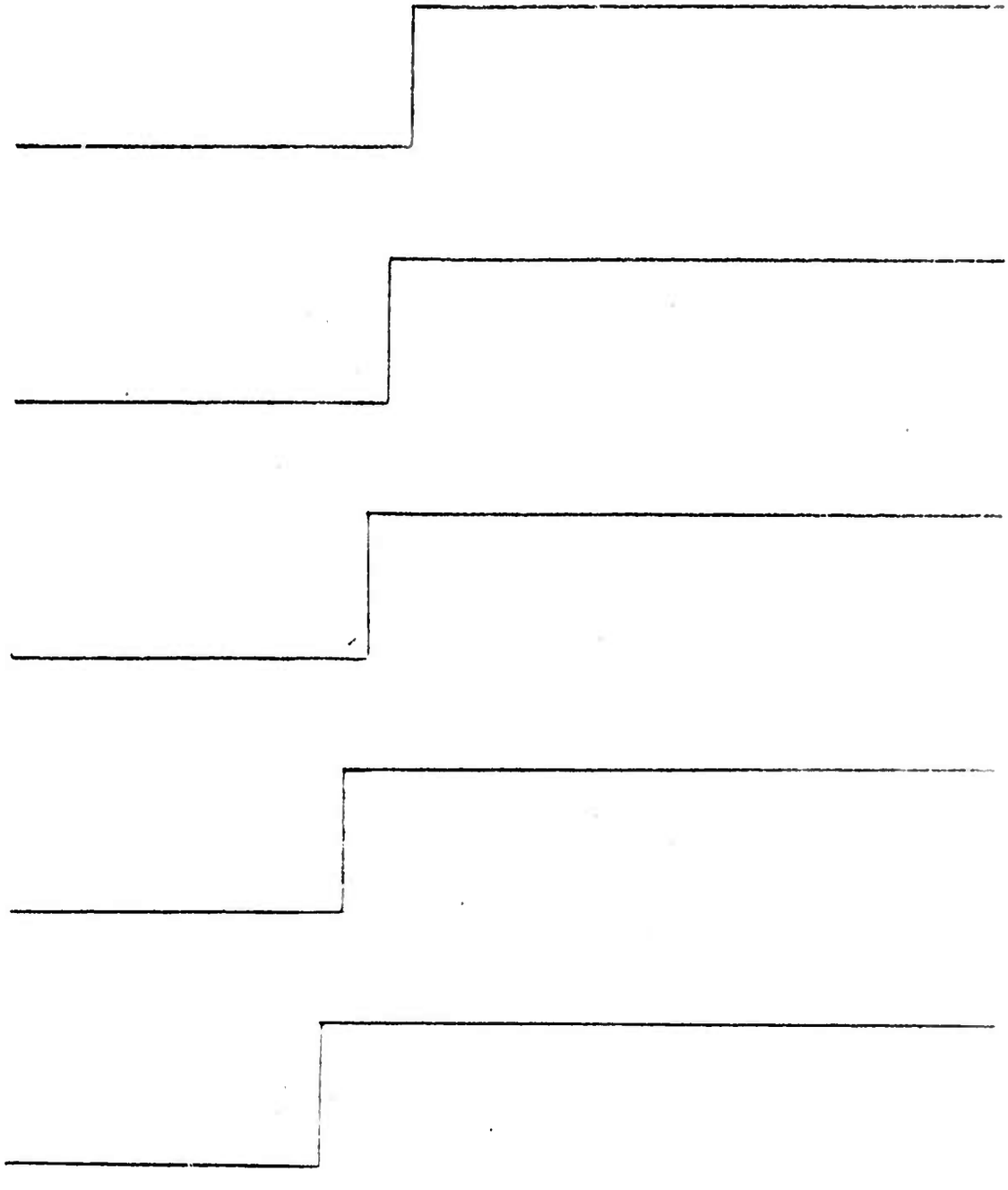

Figure 2.11a Overlay

a)

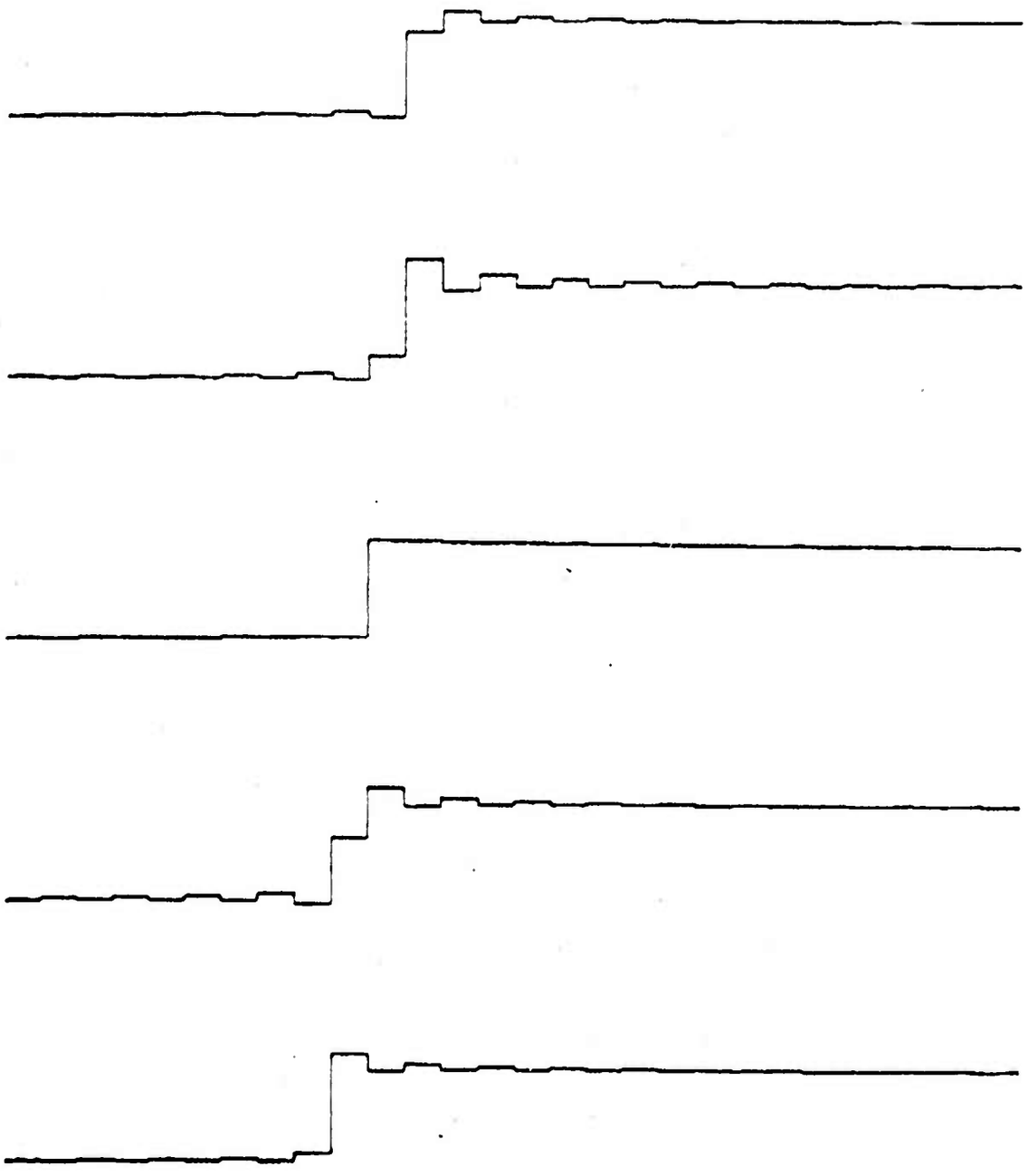

Figure 2.11 Radius vs Length for a Uniform Tube of Varying Length (Spectra Shown in Figure 2.8); Length Increment on Reconstruction = 1.0 cm. Original Tubes on Overlays.

a. Reconstructed From Uncorrected Spectra
b. Reconstructed From Corrected Spectra

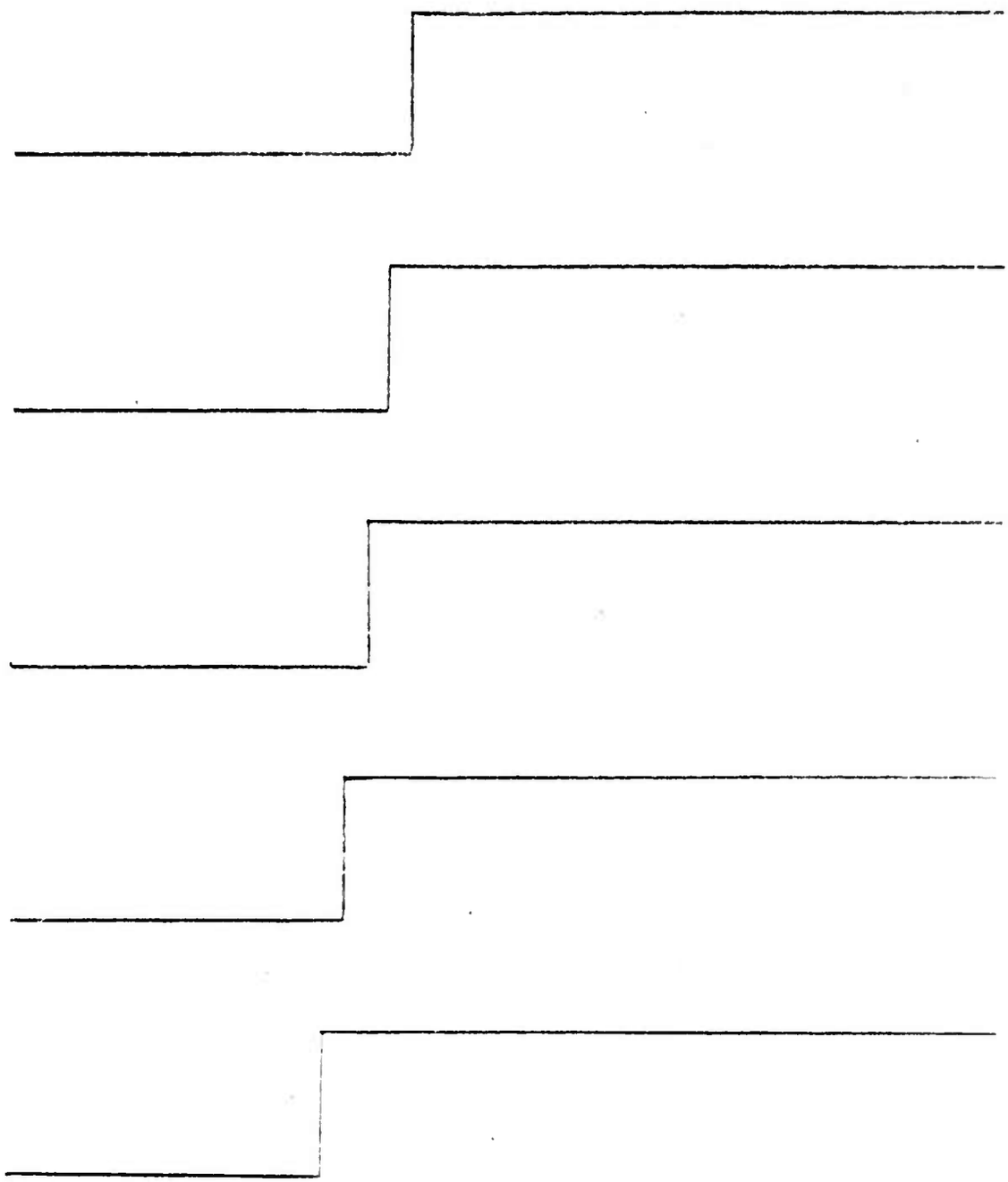

Figure 2.11b Overlay

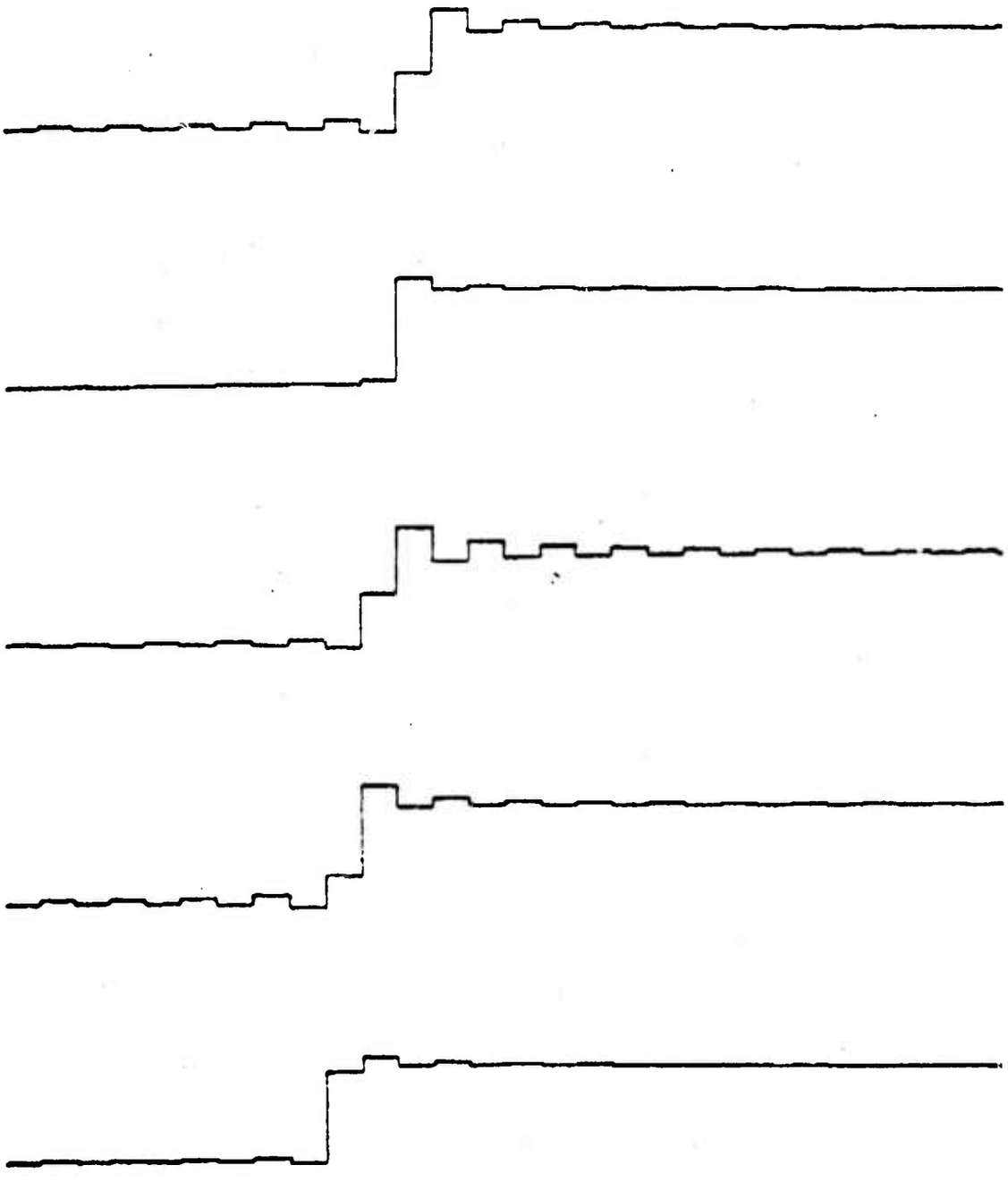

Figure 2.11b

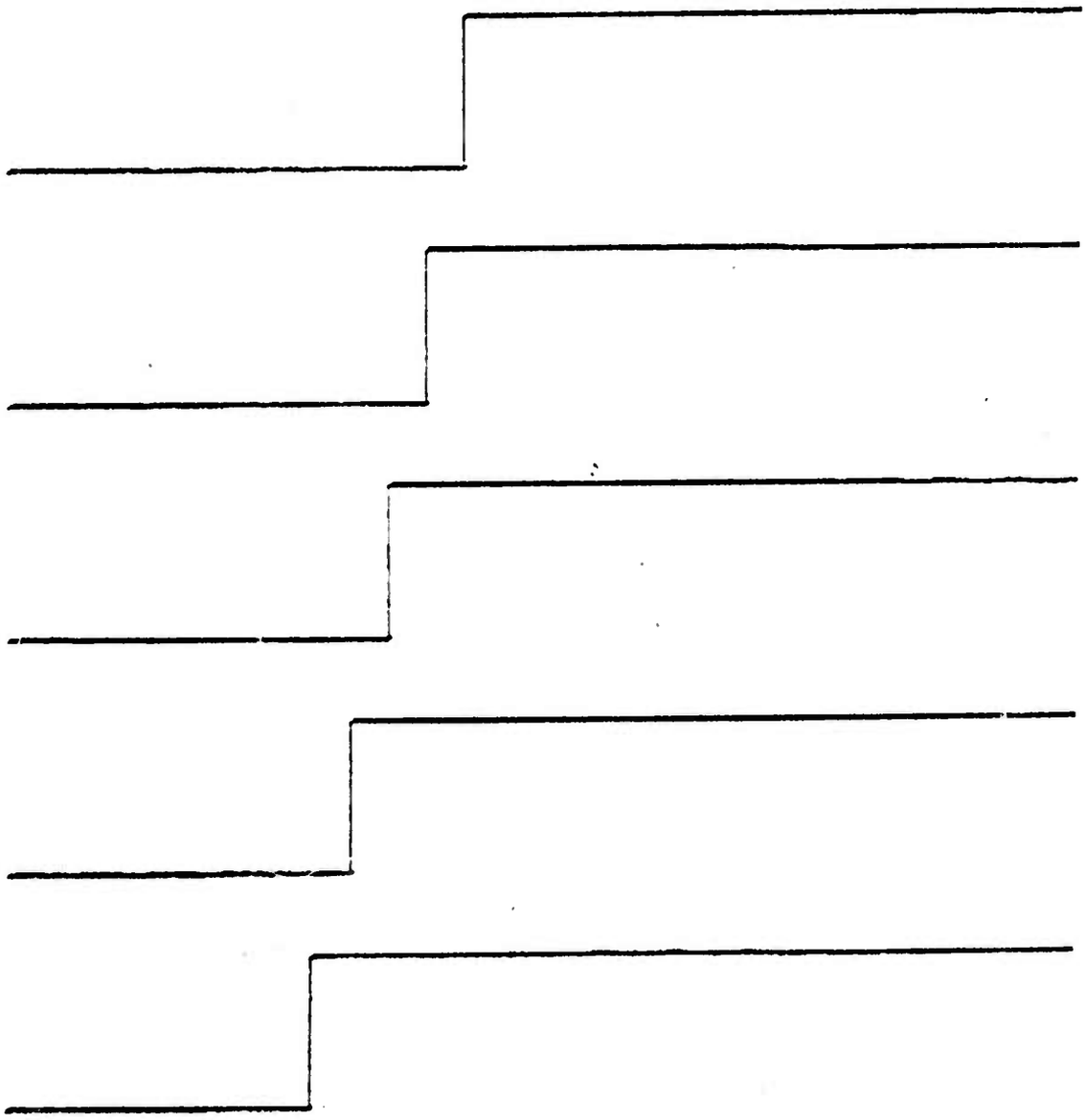

Figure 2.12a Overlay

a)

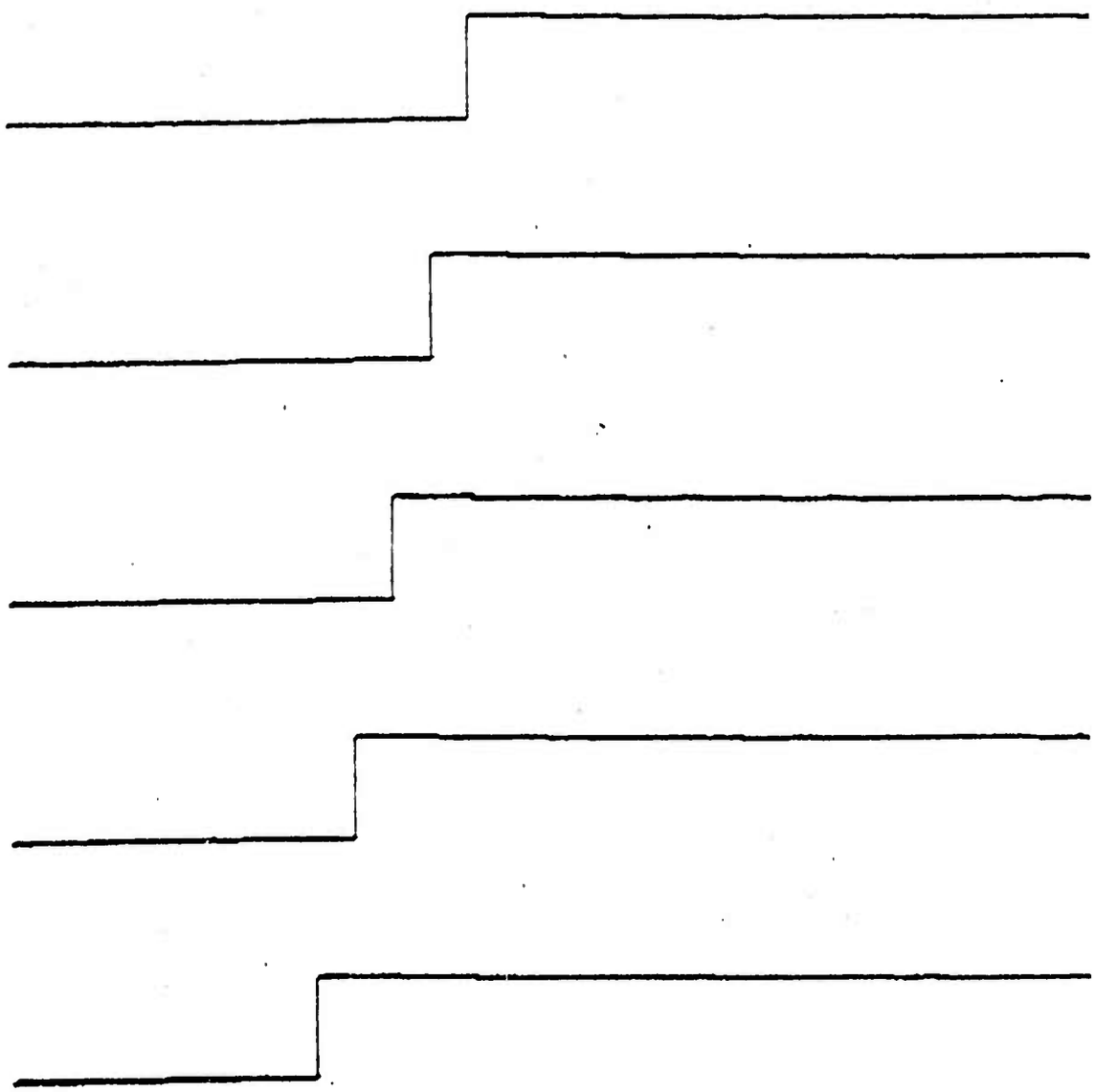

Figure 2.12 Radius vs Length for a Uniform Tube of Varying Length; Length Increment on Reconstruction = 1.7 cm. Original tubes shown on overlays.

a. Reconstructed From Uncorrected Spectra
b. Reconstructed From Corrected Spectra

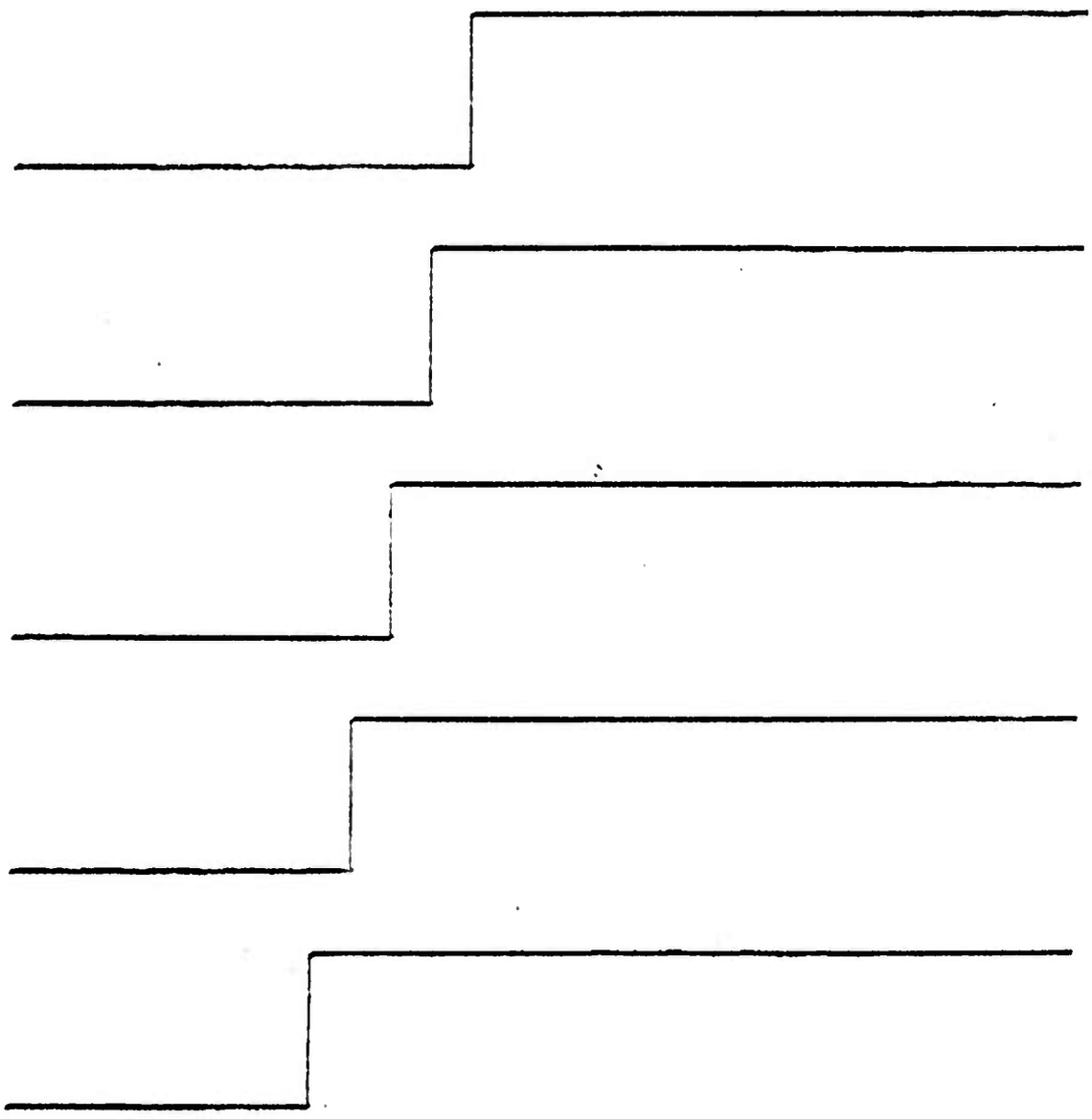

Figure 2.12b Overlay

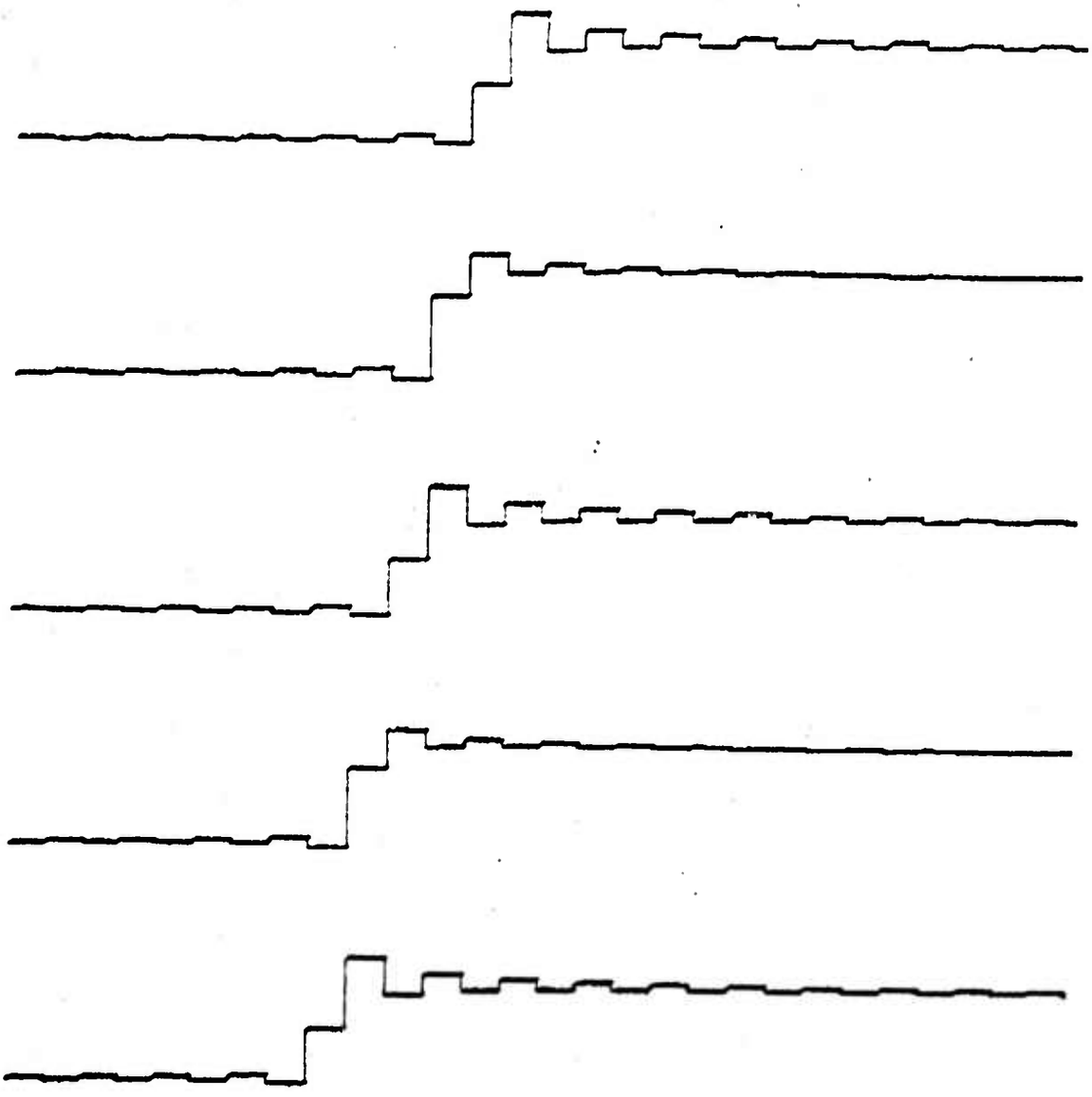

Figure 2.12b

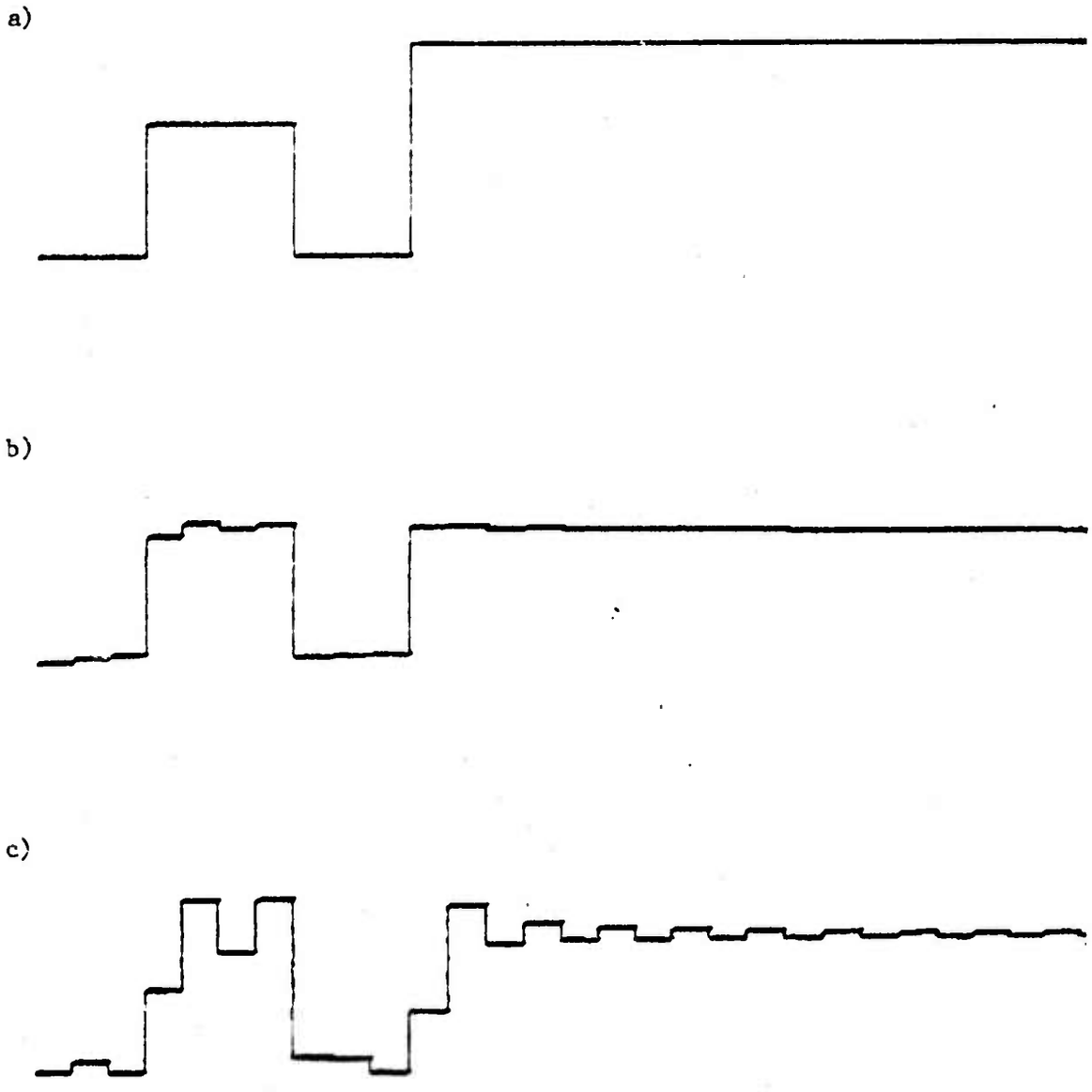

Figure 2.13 Radius vs Length for a 3 Segment Cavity with Termination (Spectra Shown in Figure 2.9)

a. Original Cavity
b. Reconstructed From Uncorrected Data
c. Reconstructed From Corrected Data

CHAPTER 3. EXPERIMENTAL RESULTS

3.1 EXPERIMENTAL APPARATUS

Figure 3.1 shows a block diagram of the apparatus for making cavity impulse response measurements. The cavity under test is fitted to 8 foot termination tubes by aluminum flanges. A speaker drives the end of one of the long tubes and a microphone in the other tube detects the cavity output signal. The peripheral electronics are briefly described here, for more detail, see the previous report on this contract (CHI-QTR-101). The speaker signal is supplied by the computer, which operates in a mode of simultaneously outputting to the speaker and reading the microphone signal. In practice a series of 64 consecutive pulses are programmatically output and the input signals are summed, resulting in a background noise reduction of 18db.

Figure 3.2 shows the signal detected at the microphone with no cavity present and the termination tubes connected to one another. The total signal shown has a duration of about 15m sec. The ringing after the pulse is an artifact of the 5kHz filter in the speaker circuit. Figure 3.3 shows a log spectrum of the source pulse from 0 to 10kHz. The sharp cut at 5kHz is the filter bandpass. As is seen here, the source spectrum is fairly flat to 5kHz, nevertheless, it is subtracted from the log spectra of cavity data to normalize out the variations in source power as a function of frequency.

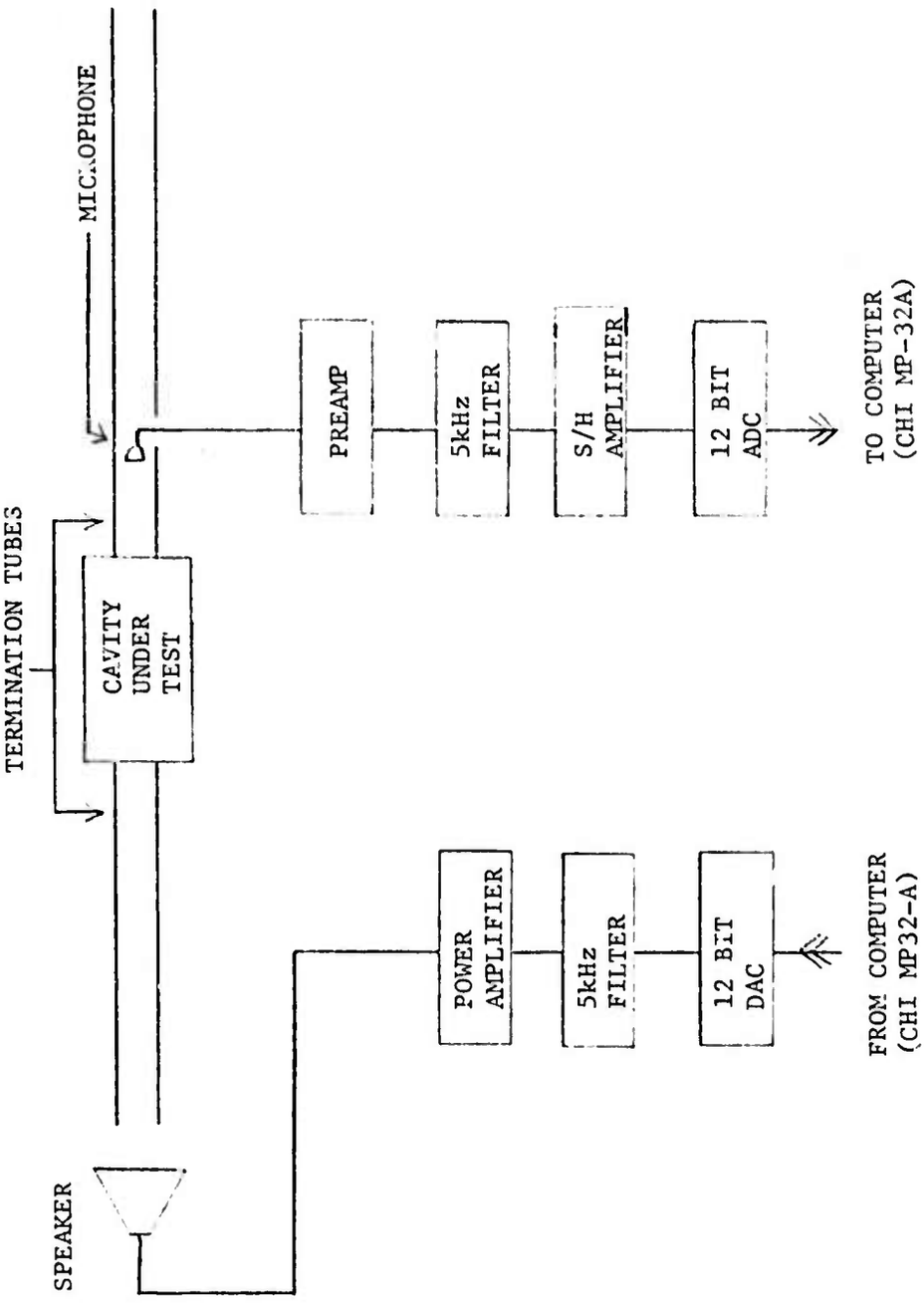

Figure 3.1 Block Diagram of Experimental Apparatus for Measuring Cavity Impulse Response

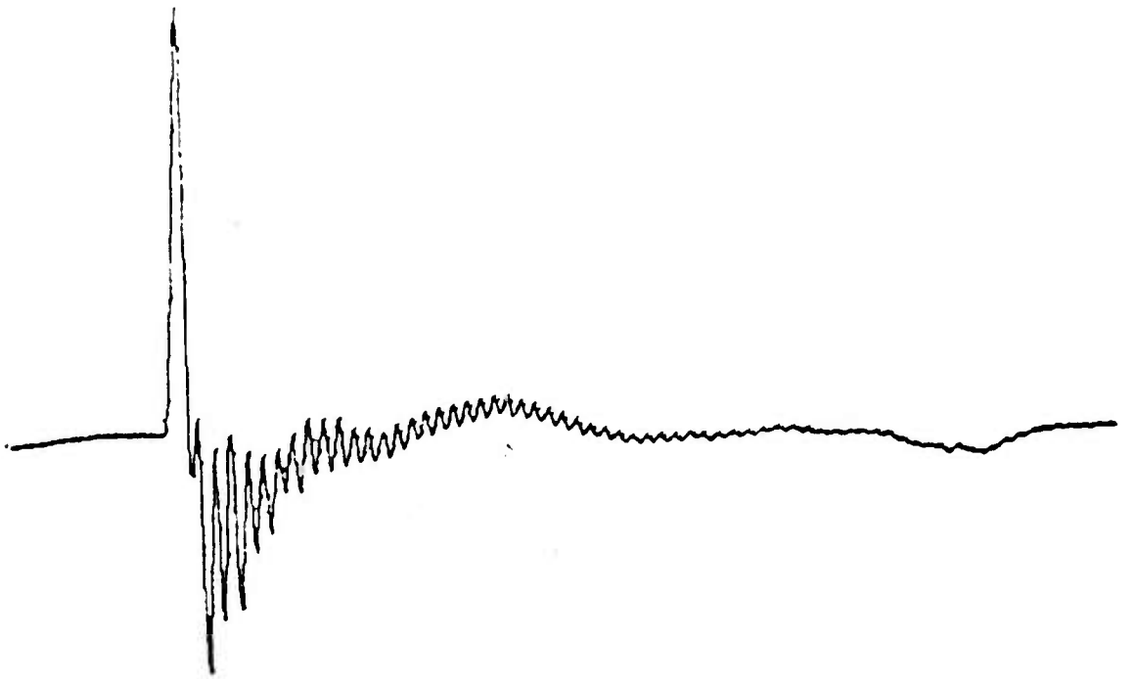

Figure 3.2 Source Impulse for Cavity Measurements

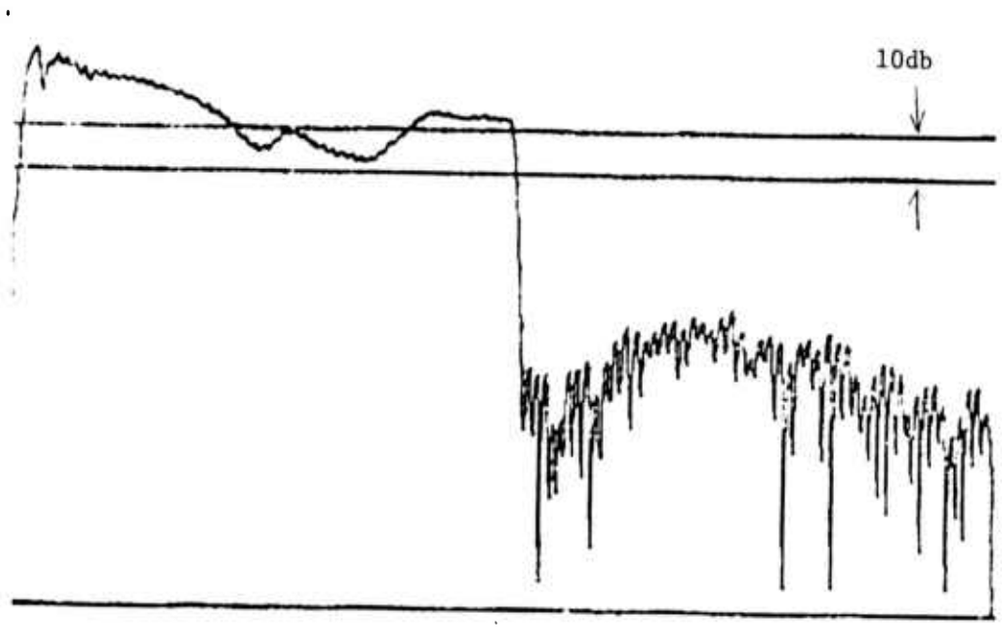

Figure 3.3 Measured Log Spectrum From 0 to 10kHz of Source Impulse

3.2 UNIFORM TUBE DATA

The most straight forward test of the apparatus is a tube of constant cross section. The measured and computed log spectra of three such tubes appear in Figure 3.4. The termination tubes for all of these measurements have radius 1.9 cm. The radii of the three measured tubes are 1.27, .794, .476 cm; all have length 17 cm. The length scale is chosen to correspond to the actual scale of the vocal tract.

Several comments can be made about the uniform tube example. The line structure is basically that of tube open at both ends (cf, Equation 1.18), however, the detailed structure is not described by this simple theory. If the data is fit with the $.8\sqrt{A}$ length correction, the lowest peak in the measured spectrum agrees with the theory. However, the higher order theoretical peaks are slightly lower in frequency than in the observed spectrum. In Figure 3.4, the observed spectra are fit with the frequency dependent length correction developed in Chapter 2. As can be seen, the agreement is good for all of the peaks. Although it is not obvious from the diagram, the tube spectra shift slightly as the tube radius changes. This shift is also apparent in the theoretical spectra, resulting in a good fit independent of tube radius.

Figure 3.5 shows the reconstructed area function of a uniform tube. The plot is actually not area function, but radius vs length. The actual cavity is drawn at the top of the Figure and two different reconstructions appear below it. All are on the same scale. The reconstructions are done by the optimal filter method described in section 2.4. The reconstruction in 3.5b is done from the actual cavity data; the reconstruction in 3.5c is done from the corrected theoretical spectrum for the tube. Neither of the reconstructions show a step at the tube mouth as large as the one in the original; this is characteristic of all of the reconstructions described in this paper. The reconstruction derived from the data is noisier and more difficult to interpret then the reconstruction derived from the theoretical spectrum. The reconstruction derived from the theory has the same length problem seen in section 2.4. The reconstruction is longer than the actual cavity because it contains information from the length corrected spectrum.

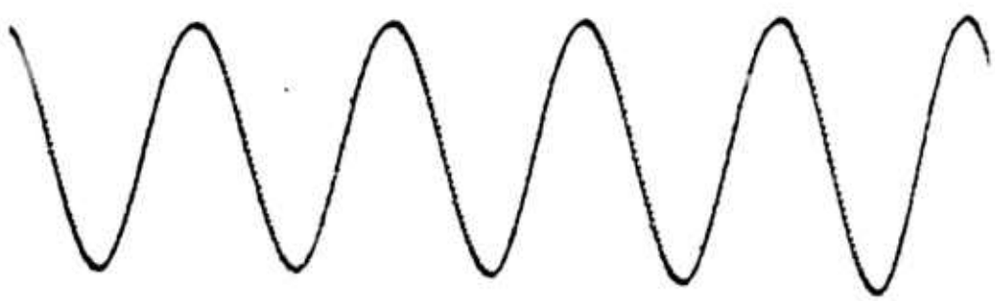

Figure 3.4a Overlay

a)

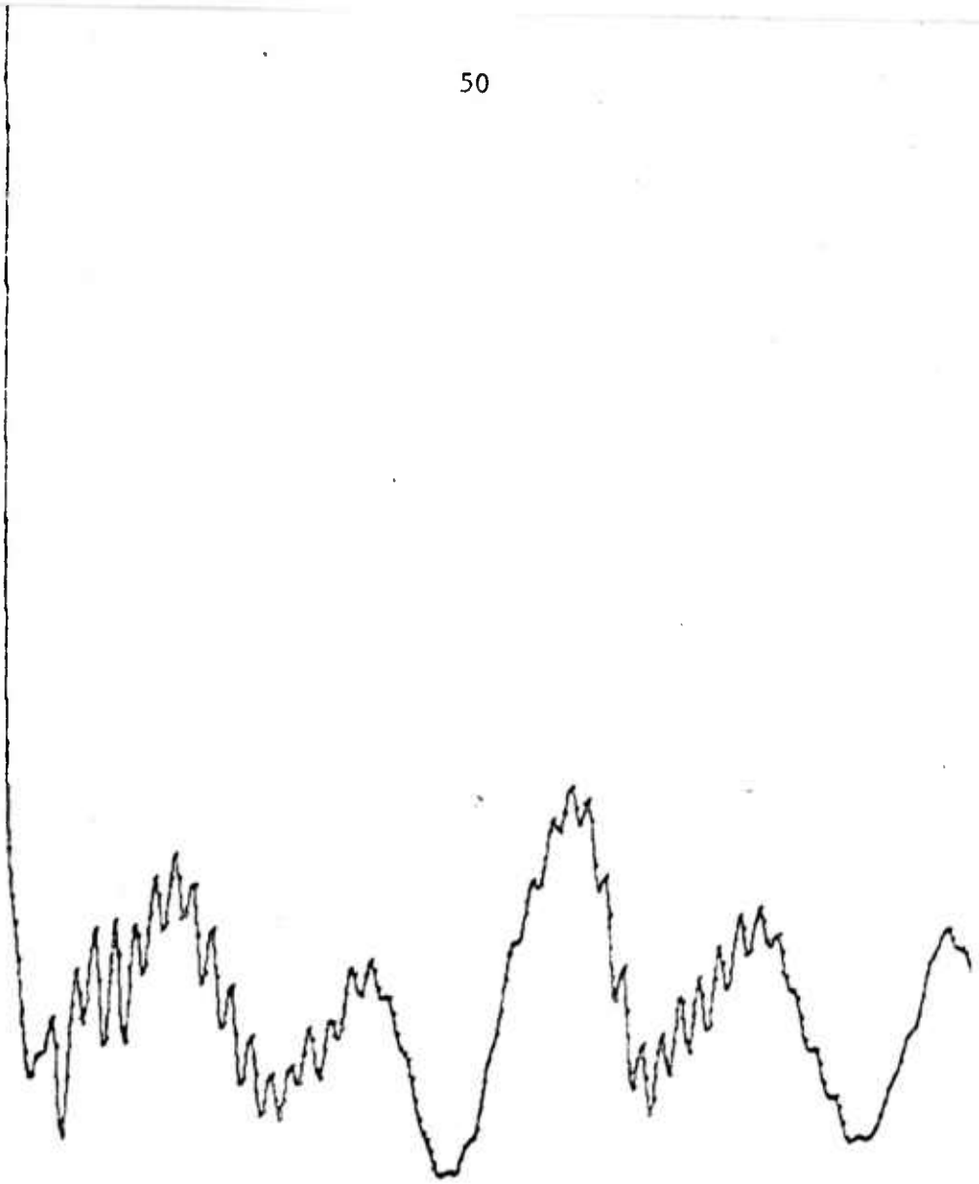

Figure 3.4 Measured Log Spectra From 0 to 5kHz of Uniform Tubes of Varying Radius with Fixed Termination. Smooth Curves on Overlays are Theoretical Spectra

a. Radius = 1.27 cm.
b. Radius = .794 cm.
c. Radius = .476 cm.

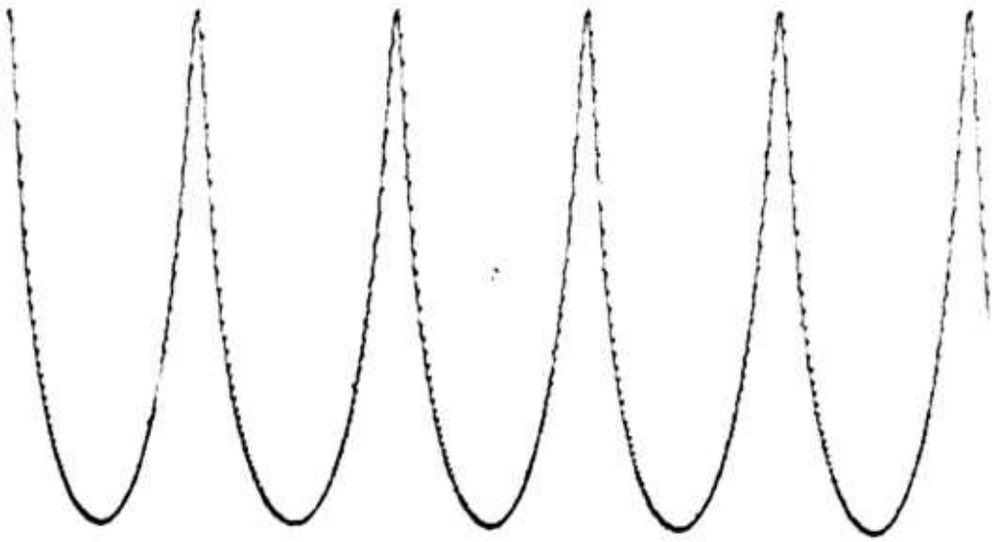

Figure 3.4b Overlay

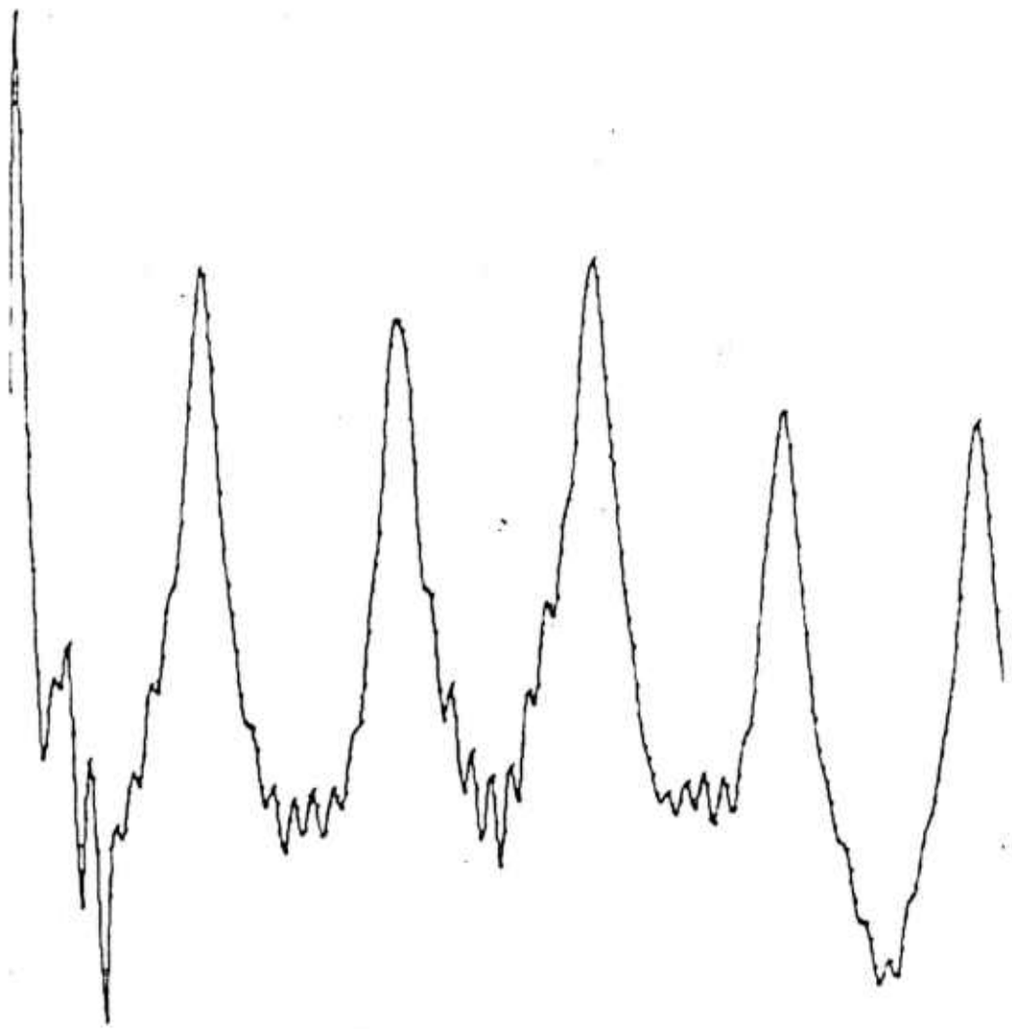

Figure 3.4b

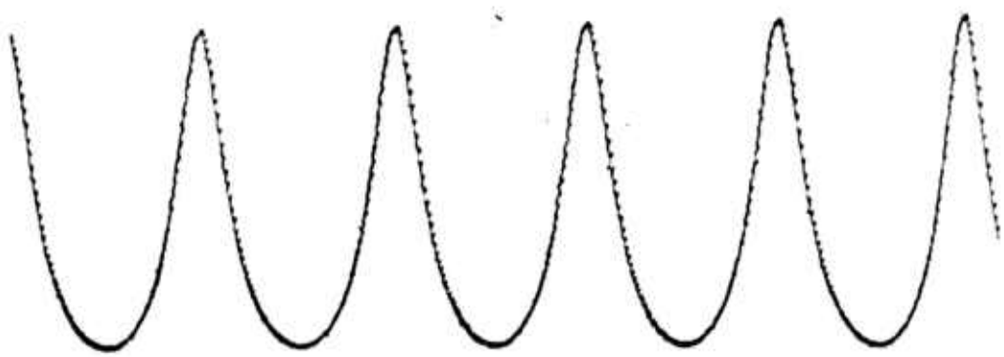

Figure 3.4c Overlay

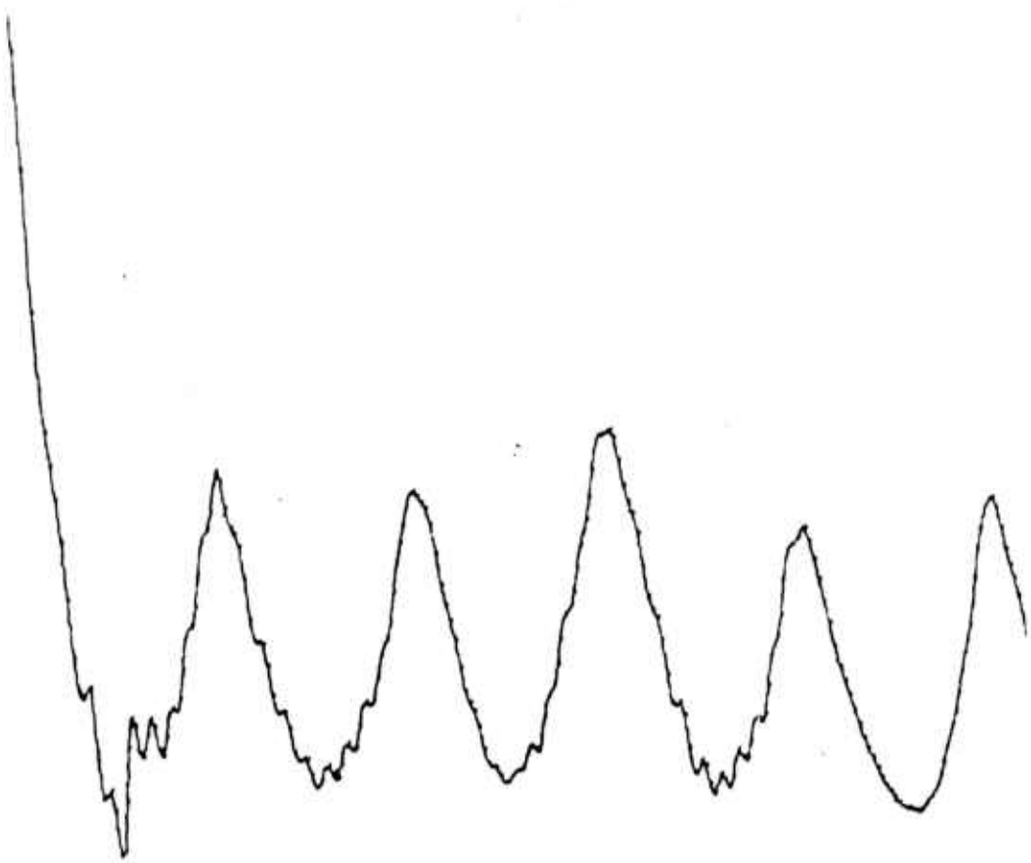

Figure 3.4c

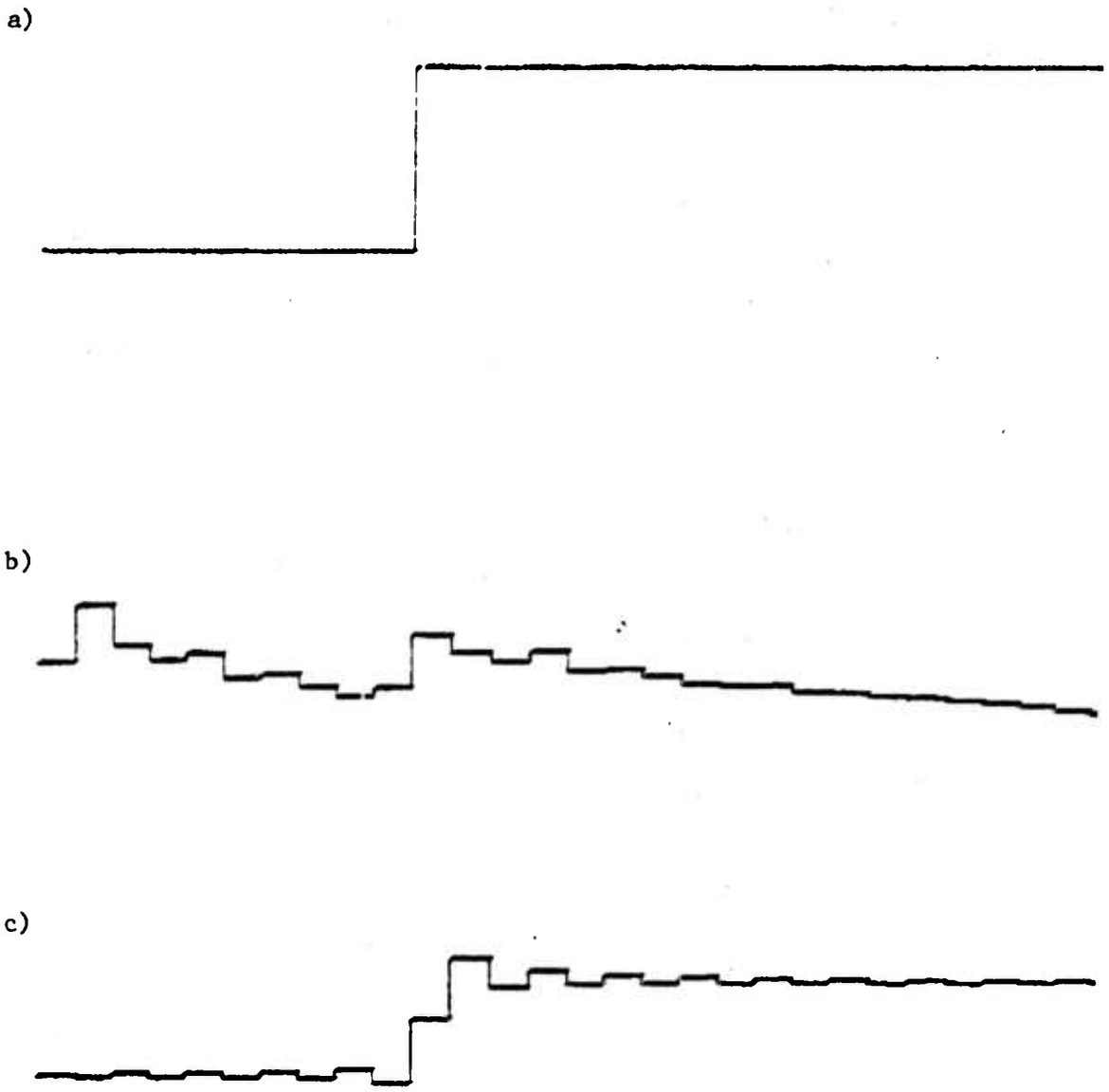

Figure 3.5 Radius vs Length for Uniform Tube
a. Actual Tube
b. Reconstructed From Data
c. Reconstructed From Theoretical Spectrum

Figure 3.6 shows the measured and calculated log spectra of a uniform aperture placed between the termination tubes. The aperture has a length of .7 cm. and a radius of .31 cm. As expected, the spectrum shows a broad decreasing profile from 0Hz to 5kHz. This system is just a very short uniform tube, so the spectrum here is approaching the first minimum between the 0Hz peak and the first non-zero resonance.

Figure 3.7 shows the area function of the aperture reconstructed from the data and from the theoretical spectrum. At the top of the figure is the original aperture. All area functions are on the same scale. The comments made about Figure 3.5 also apply to this case.

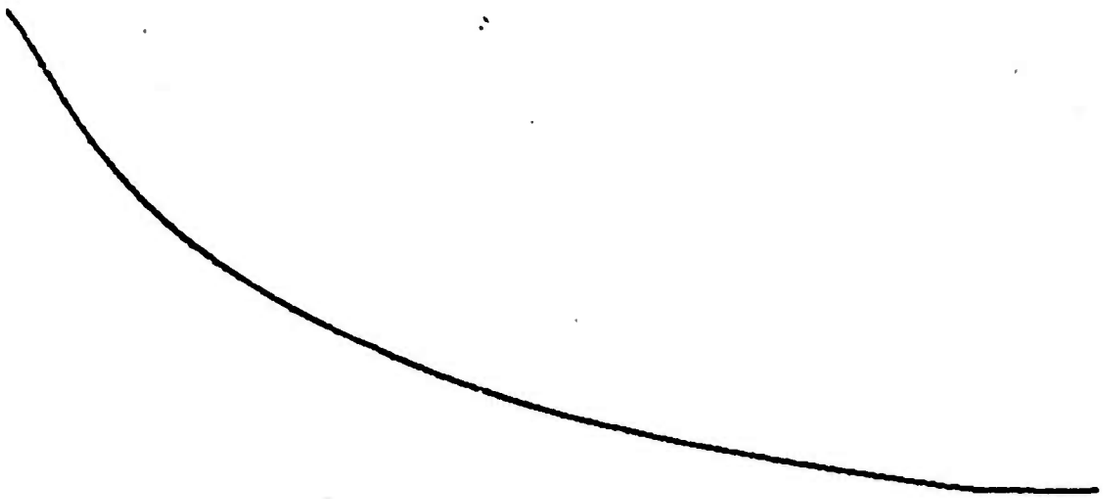

Figure 3.6 Overlay

Figure 3.6 Measured Log Spectrum From 0 to 5kHz of Aperture. Smooth Curve on Overlay is Theoretical Spectrum

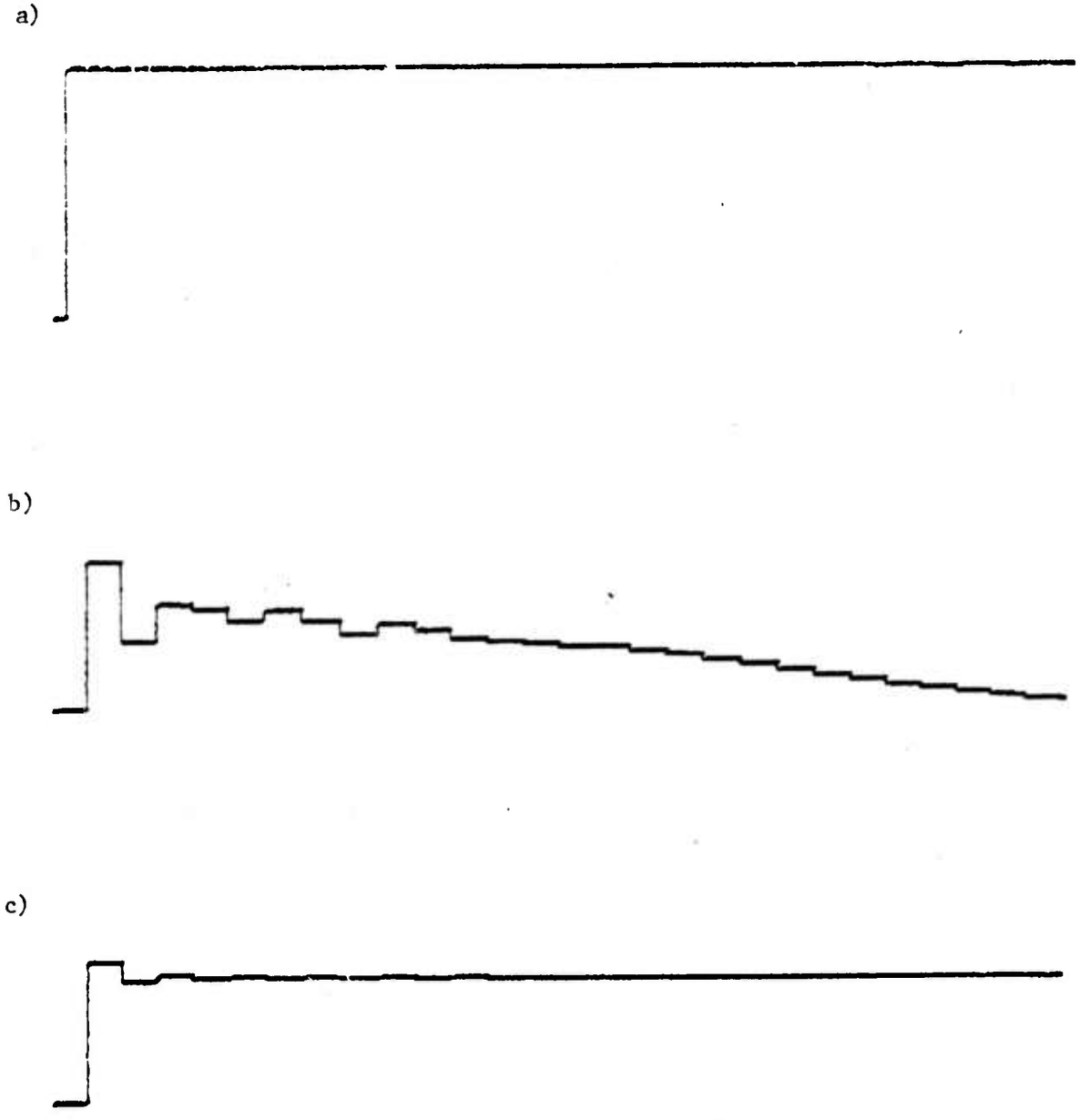

Figure 3.7 Radius vs Length for Aperture
a. Actual Aperture
b. Reconstructed From Data
c. Reconstructed From Theoretical Spectrum

3.3 STEPPED CAVITY DATA

In the previous section, area functions are derived for uniform tubes with terminations. In this section terminated cavities with varying cross section are considered.

Figure 3.8 shows the measured log spectrum from 0 to 5kHz for a uniform tube of length 17 cm. and radius .775 cm. with an aperture at the input. The aperture has length .7 cm. and radius .31 cm. Both termination tubes have radius 1.9 cm. The spectrum, as expected, looks like the product of the aperture and the uniform tube. That is, the strong resonant structure of the tube is modulated by the broad rolloff of the aperture. The smooth curve on the overlay is a fit of the data computed from Equation 2.16.

Figure 3.9 shows the above mentioned tube with aperture at input and the derived area functions. The first derived area is from the data and the second from the theoretical fit to the data. Notice how difficult the interpretation of the area derived from the data would be without a priori knowledge of the actual structure.

Figure 3.10 shows the log spectrum, measured and calculated, from 0Hz to 5kHz for a three segment terminated cavity. The cavity and the derived area functions are shown in Figure 3.11. As before, the theoretical spectrum is a good fit to the data, and the theoretically derived area function is much easier to interpret than the area function derived from the data.

Figures 3.12 and 3.13 show the log spectrum and area function for the stepped cavity of the previous example with an aperture at the input. The features are qualitative by the same as in the previous cases. That is, unless a priori knowledge is available, the interpretation of the area function derived from the data is not obvious.

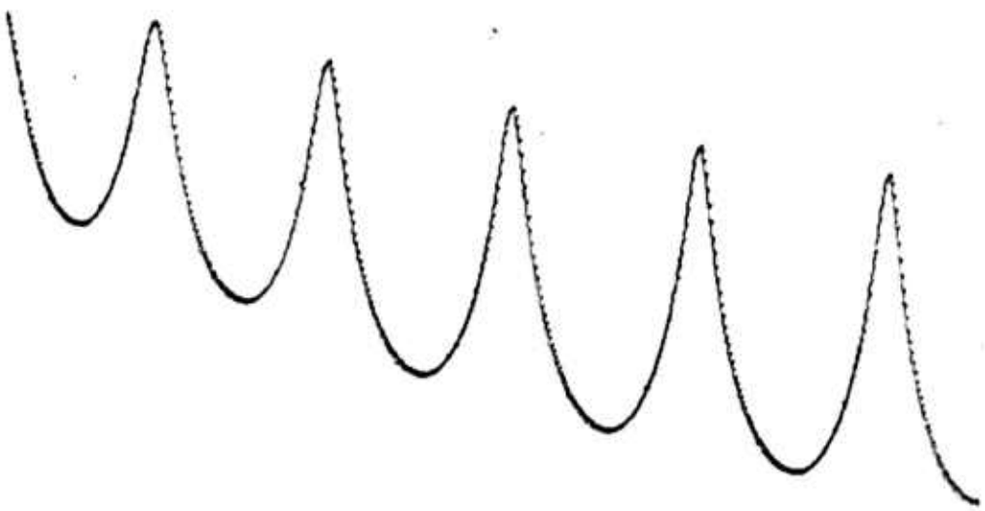

Figure 3.8 Overlay

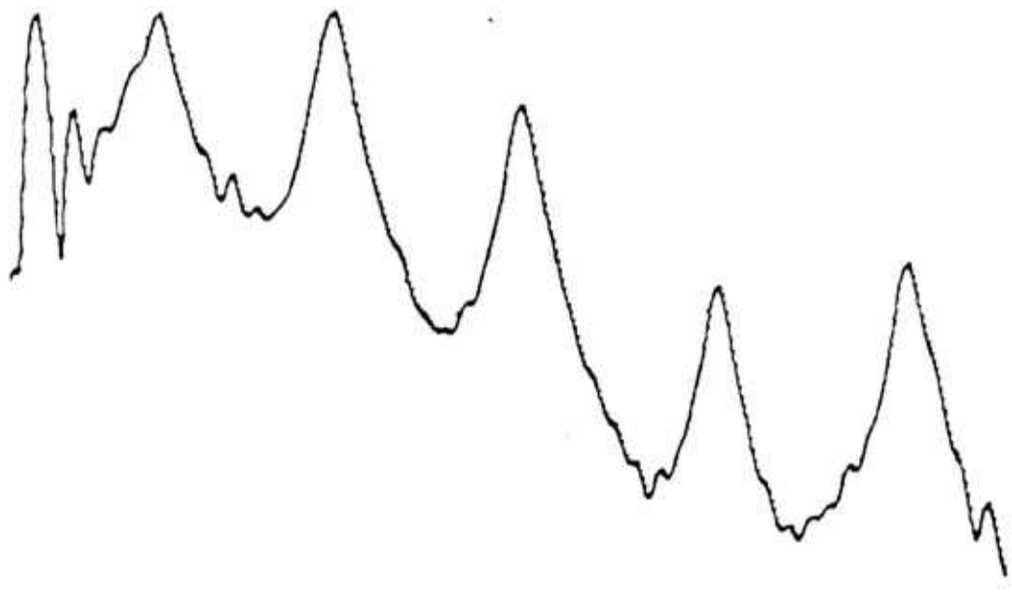

Figure 3.8 Measured Log Spectrum From 0 to 5kHz of Uniform Tube with Aperture at Input. Smooth Curve on Overlay is Theoretical Spectrum

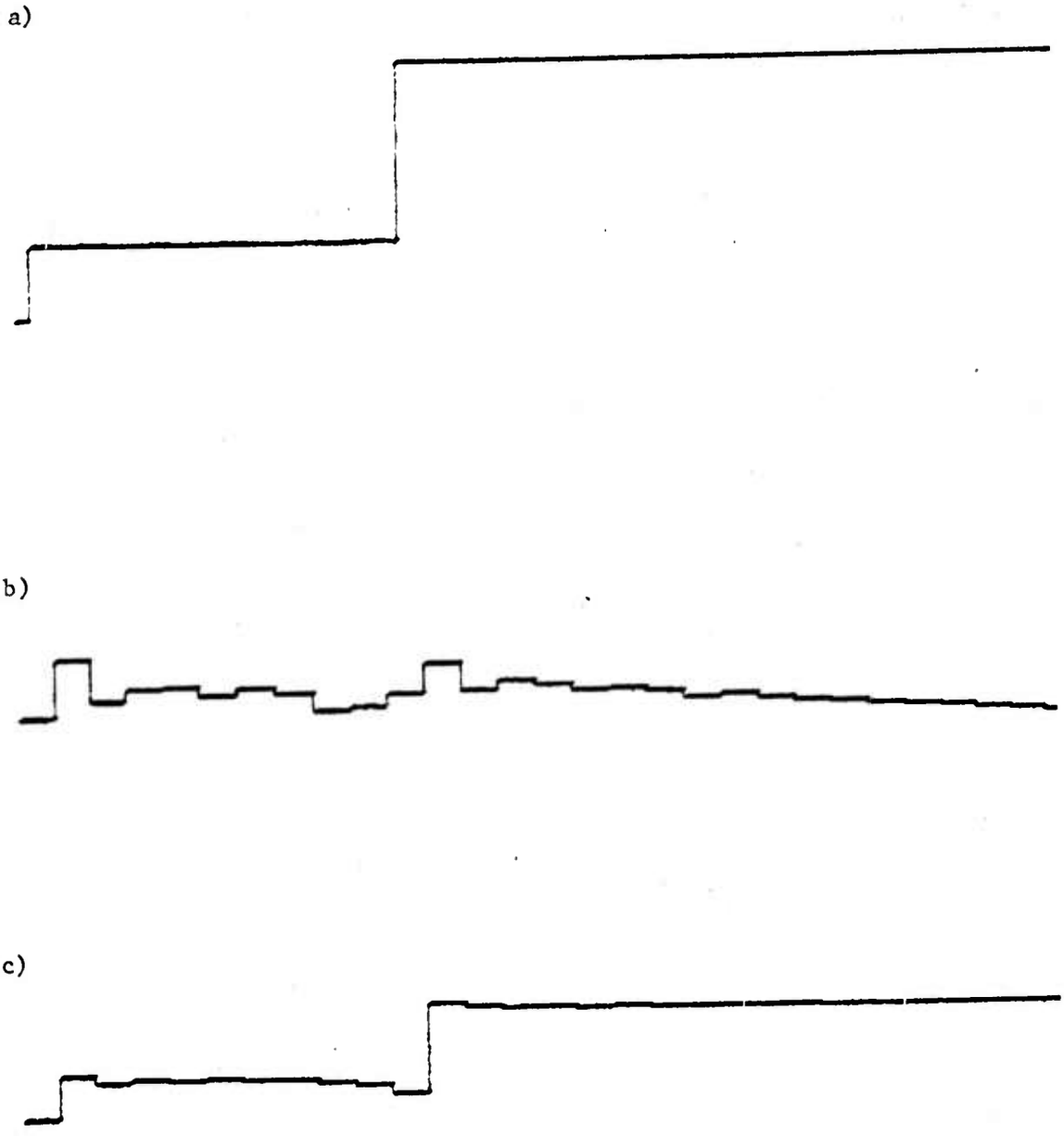

Figure 3.9 Radius vs Length for Uniform Tube with Aperture at Input

a. Actual Cavity
b. Reconstructed From Data
c. Reconstructed From Theoretical Spectrum

Figure 3.10 Overlay

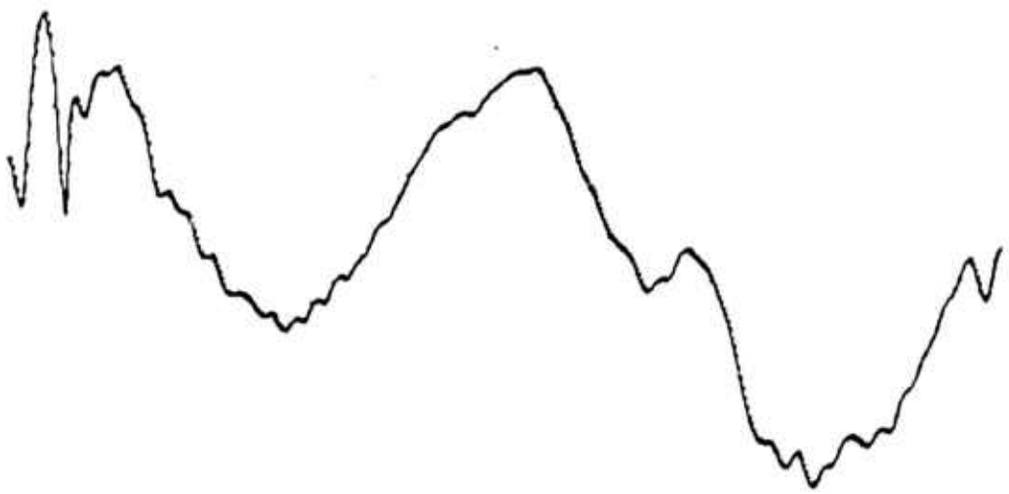

Figure 3.10 Measured Log Spectrum From 0 to 5kHz of Stepped Cavity. Smooth Curve on Overlay is Theoretical Spectrum

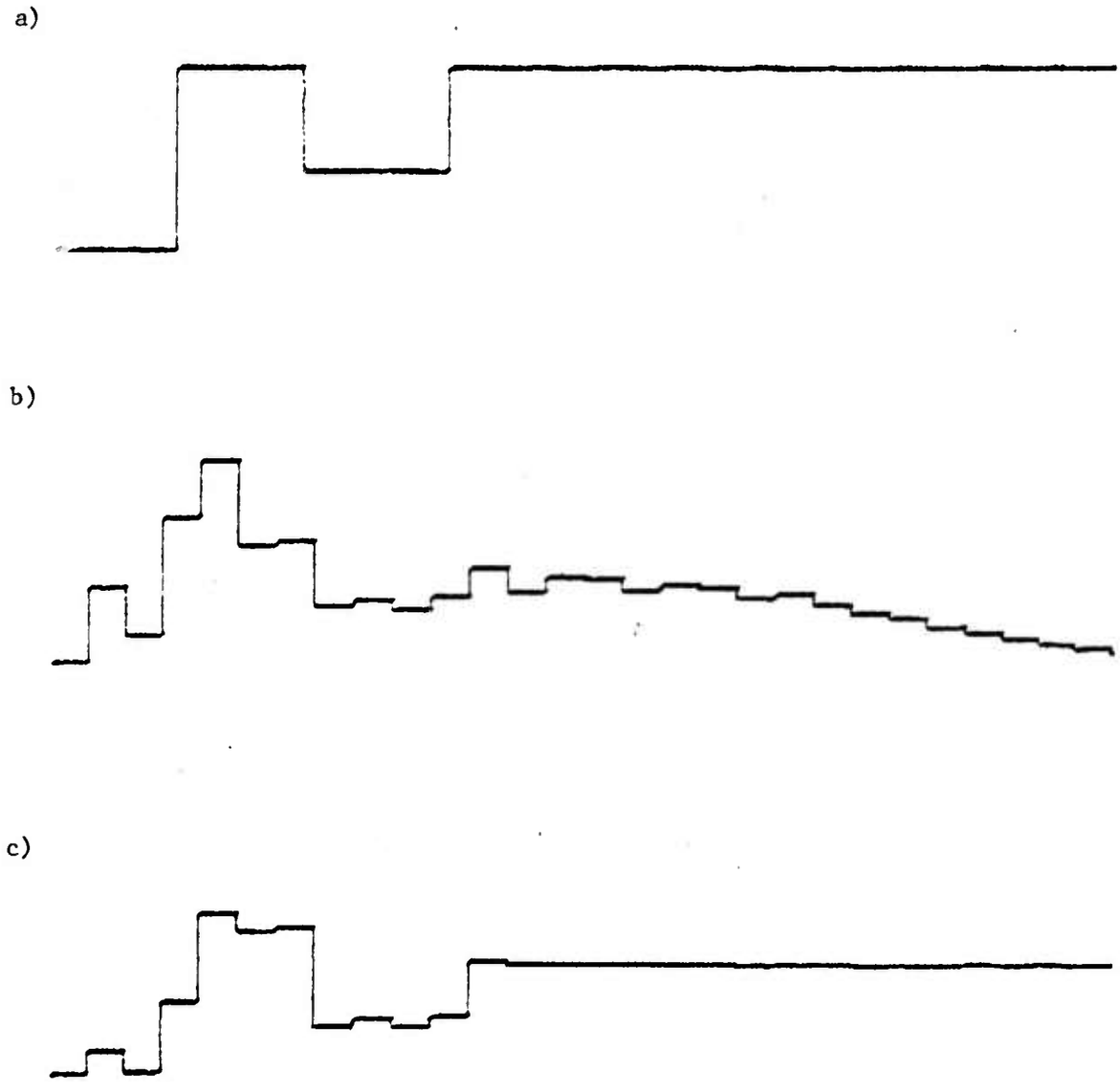

Figure 3.11 Radius vs Length for Stepped Cavity
a. Actual Cavity
b. Reconstructed From Data
c. Reconstructed From Theoretical Spectrum

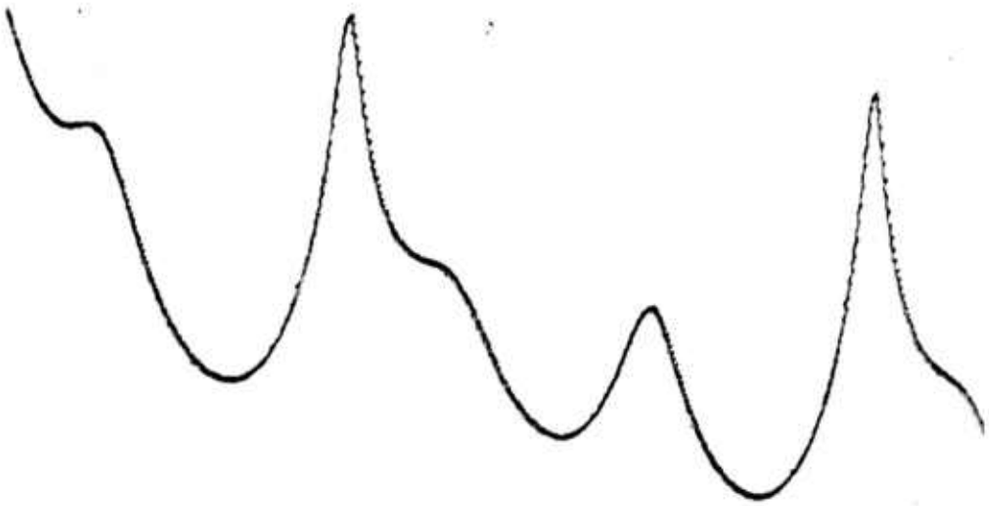

Figure 3.12 Overlay

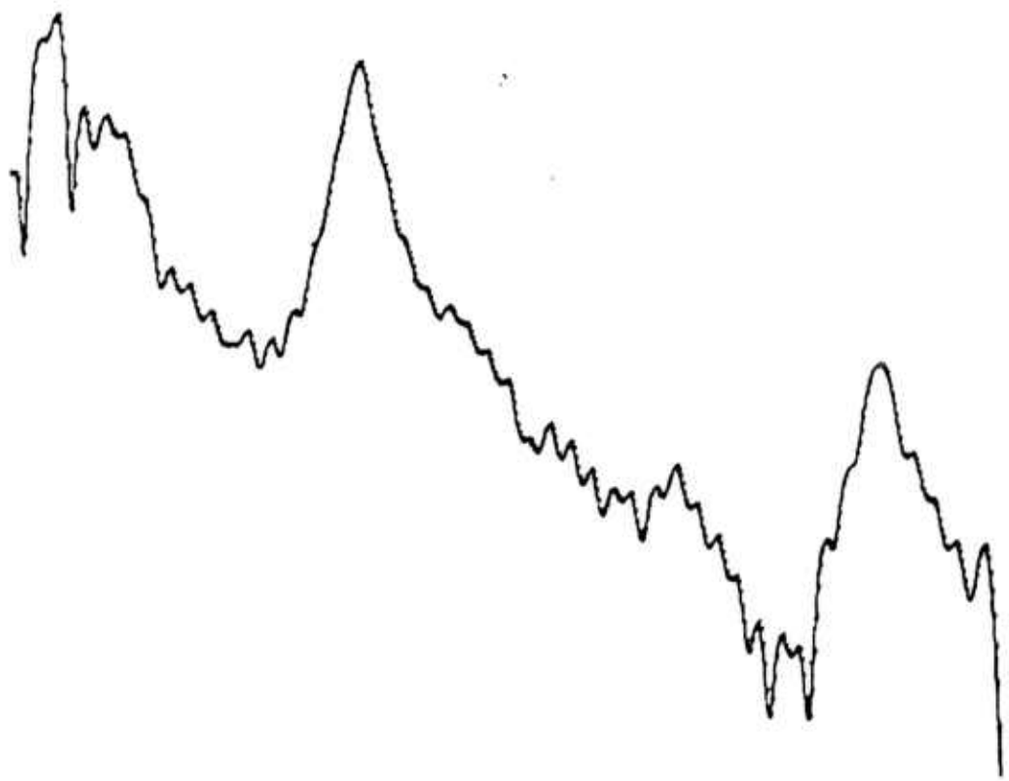

Figure 3.12 Measured Log Spectrum From 0 to 5kHz of Stepped Cavity with Pinch at Input. Smooth Curve on Overlay is Theoretical Spectrum

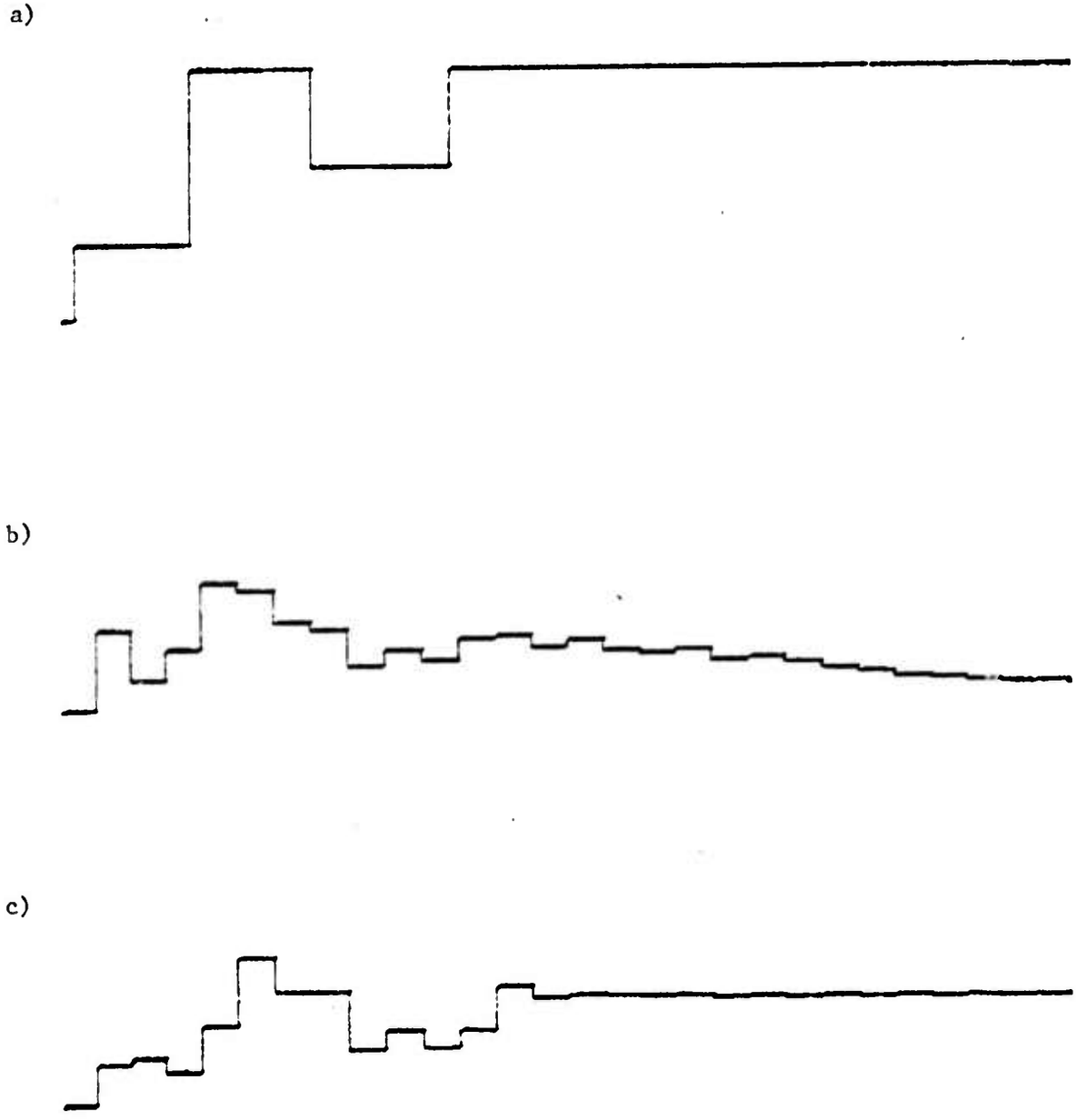

Figure 3.13 Radius vs Length for Stepped Cavity with Aperture at Input

a. Actual Cavity
b. Reconstructed From Data
c. Reconstructed From Theoretical Spectrum

CHAPTER 4: CONCLUSIONS

An experimental investigation of the optimal filter as an area function predictor has been performed. The impulse response is measured for several different cavities, all composed of segments of circular cross section. From this information, the transmission spectrum is computed. The autocorrelation function is computed from the spectrum and the optimal filter is found recursively by the method of Levinson. The filter coefficients are then converted to an area function which is compared to the area function of the original cavity. A model presented to explain the observed spectra includes a general length correction for a cavity constructed of segments with circular cross section. The cavity area function is also computed from the theoretically derived spectrum of the original cavity. In addition, the area functions of several hypothetical cavities are computed from their theoretically derived spectra.

The accuracy of the optimal filter area prediction is found to depend on the step length implicit in the filter computation. If the actual cavity has lengths in it which are multiples of the step, then the fit is fairly good. In other more general cases, the fit does not work out as well. It is also found that the area functions predicted from data are longer than the original cavities. This occurs because each cross section discontinuity in the cavity contributes an effective extra length to the cavity, so the cavity appears longer in the data.

It is felt that a more complete statistical error analysis is needed to assign confidence levels to the technique as applied to speech data. It may also be possible to better predict the area function of a cavity if an inverse length correction can be made in the optimal filter calculation. The optimal filter area function predictor may find application in fields other than speech research but its performance characteristics must be carefully documented and understood before this can easily occur.

REFERENCES

1. H.K. Dunn, J. Acoust. Soc. Am. 22, 740(1950).

2. P. Mermelstein, J. Acoust. Soc. Am. 41, 1283(1967).

3. M.R. Schroeder, J. Acoust. Soc. Am. 41, 1002(1967).

4. B. Gopineth and M.M. Sondhi, Bell Syst. Tech. Jour. 49, 1195(1970).

5. A. Paige and V.W. Zue, IEEE Trans. Aud. and Elec. Acoust., AU-18, 7(1970).

6. B.S. Atal and S.L. Hanauer, J. Acoust. Soc. Am. 50, 637(1971).

7. H. Wakita, SCRL Monograph 9, 1972.

8. John D. Markel and A.H. Gray, Jr., IEEE Trans. Aud. and Elec. Acoust., AU-21, 69(1973).

9. John D. Markel and A.H. Gray, Jr., IEE Trans. Aud. and Elec. Acoust., ASSP-22, 124(1974).

10. B.S. Atal, J. Acoust. Soc. Am. 55, 1304(1974).

11. F.C. Karal, J. Acoust. Soc. Am. 25, 327(1953).

12. A.G. Webster, Proc. Natl. Acad. Sci. (U.S.) 5, 272(1919).

13. P.M. Morse, Vibration and Sound, McGraw-Hill, New York, 1948.

14. H. Levine and J. Schwinger, Phys. Rev. 73, 383(1948).

APPENDIX 1: FLOW CHART FOR CAVITY SPECTRUM CALCULATION

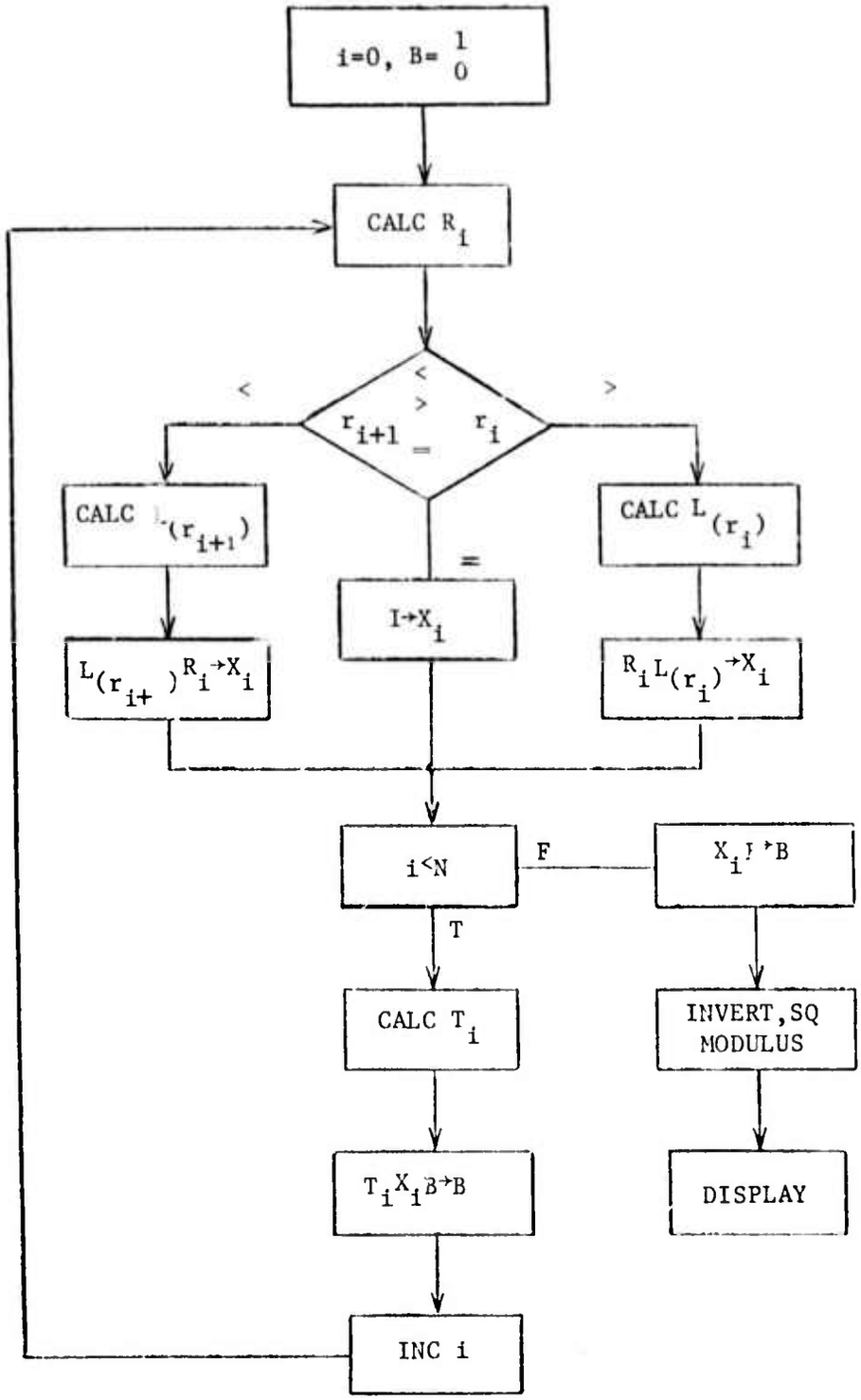

Figure A-1 Flow Chart for Cavity Spectrum Calculation